Check for updates

Accelerated RNA detection using tandem CRISPR nucleases

Tina Y. Liu [1,2], Gavin J. Knott [1,2,3], Dylan C. J. Smock[1,2], John J. Desmarais [1], Sungmin Son[4], Abdul Bhuiya[4,5], Shrutee Jakhanwal[1,2], Noam Prywes [2], Shreeya Agrawal[2,4], María Díaz de León Derby[4,5], Neil A. Switz [6], Maxim Armstrong[7], Andrew R. Harris[4], Emeric J. Charles[1], Brittney W. Thornton[1], Parinaz Fozouni [8,9,10,11], Jeffrey Shu[8,11], Stephanie I. Stephens [8,11], G. Renuka Kumar[8,11], Chunyu Zhao[8,12], Amanda Mok [13], Anthony T. Iavarone[14], Arturo M. Escajeda [15], Roger McIntosh[15], Shineui Kim[1,2], Eli J. Dugan [1,2], IGI Testing Consortium*, Katherine S. Pollard [8,12,16], Ming X. Tan[15], Melanie Ott [8,11], Daniel A. Fletcher [4,5,12,17], Liana F. Lareau [2,4], Patrick D. Hsu [2,4,13,17,18 ✉], David F. Savage [1,2 ✉] and Jennifer A. Doudna [1,2,7,17,19,20,21 ✉]

Direct, amplification-free detection of RNA has the potential to transform molecular diagnostics by enabling simple on-site analysis of human or environmental samples. CRISPR–Cas nucleases offer programmable RNA-guided RNA recognition that triggers cleavage and release of a fluorescent reporter molecule, but long reaction times hamper their detection sensitivity and speed. Here, we show that unrelated CRISPR nucleases can be deployed in tandem to provide both direct RNA sensing and rapid signal generation, thus enabling robust detection of ~30 molecules per µl of RNA in 20 min. Combining RNA-guided Cas13 and Csm6 with a chemically stabilized activator creates a one-step assay that can detect severe acute respiratory syndrome coronavirus 2 (SARS-CoV-2) RNA extracted from respiratory swab samples with quantitative reverse transcriptase PCR (qRT–PCR)-derived cycle threshold (C_t) values up to 33, using a compact detector. This Fast Integrated Nuclease Detection In Tandem (FIND-IT) approach enables sensitive, direct RNA detection in a format that is amenable to point-of-care infection diagnosis as well as to a wide range of other diagnostic or research applications.

Current strategies for RNA detection in clinical samples based on qRT–PCR provide high sensitivity (limit of detection of ~1 molecule per µl) but are too complex to implement for rapid point-of-care testing, an essential component of pandemic control[1–3]. CRISPR–Cas proteins offer a simpler alternative to PCR-based methods due to their programmable, RNA-guided recognition of RNA sequences[4–6]. Detection takes advantage of the intrinsic enzymatic functions of CRISPR–Cas proteins from type III and type VI CRISPR–Cas systems, including the multisubunit effector Csm/Cmr or the single-protein effector Cas13 (refs. [7–10]). Target RNA recognition by the effector triggers multiple-turnover *trans*-cleavage of single-stranded RNA (ssRNA) by either the same protein, in the case of Cas13, or by a separate protein called Csm6, in the case of Csm/Cmr[7,8,11,12]. Enzymatic RNA cleavage generates a fluorescent signal when directed toward a reporter oligonucleotide containing a dye and quencher pair[7,8,13]. Cas13 or Csm/Cmr is capable of reaching an RNA detection sensitivity in the attomolar range in under an hour when coupled to a target sequence amplification procedure, such as reverse transcription recombinase polymerase amplification (RT–RPA) or reverse transcription loop-mediated isothermal amplification (RT–LAMP)[7–10,14,15]. However, addition of RT–LAMP to CRISPR-based detection requires multiple liquid handling steps and/or high-temperature incubation (55–65 °C), procedures that are challenging to implement for point-of-care testing[9,10,16–18]. RT–RPA can be combined with *Leptotrichia wadei* Cas13a (LwaCas13a) detection in a single step, but the single-step assay exhibits a reduced sensitivity compared to the two-step assay, likely due to differences in optimal buffer and salt conditions for the enzymes in each step[19,20]. We reported that amplification-free RNA detection using *L. buccalis* Cas13a (LbuCas13a) with three guide RNAs could rapidly identify

[1]Department of Molecular and Cell Biology, University of California, Berkeley, Berkeley, CA, USA. [2]Innovative Genomics Institute, University of California, Berkeley, Berkeley, CA, USA. [3]Monash Biomedicine Discovery Institute, Department of Biochemistry & Molecular Biology, Monash University, Victoria, Australia. [4]Department of Bioengineering, University of California, Berkeley, Berkeley, CA, USA. [5]UC Berkeley, UC San Francisco Graduate Program in Bioengineering, University of California, Berkeley, Berkeley, CA, USA. [6]Department of Physics and Astronomy, San José State University, San José, CA, USA. [7]Molecular Biophysics and Integrated Bioimaging Division, Lawrence Berkeley National Laboratory, Berkeley, CA, USA. [8]Gladstone Institute of Virology, Gladstone Institutes, San Francisco, CA, USA. [9]Medical Scientist Training Program, University of California, San Francisco, San Francisco, CA, USA. [10]Biomedical Sciences Graduate Program, University of California, San Francisco, San Francisco, CA, USA. [11]Department of Medicine, University of California, San Francisco, San Francisco, CA, USA. [12]Chan-Zuckerberg Biohub, San Francisco, CA, USA. [13]Center for Computational Biology, University of California, Berkeley, Berkeley, CA, USA. [14]QB3/Chemistry Mass Spectrometry Facility, University of California, Berkeley, Berkeley, CA, USA. [15]Wainamics Inc., Pleasanton, CA, USA. [16]Department of Epidemiology & Biostatistics, University of California, San Francisco, San Francisco, CA, USA. [17]California Institute for Quantitative Biosciences (QB3), University of California, Berkeley, Berkeley, CA, USA. [18]Berkeley Stem Cell Center, University of California, Berkeley, Berkeley, CA, USA. [19]Howard Hughes Medical Institute, University of California, Berkeley, Berkeley, CA, USA. [20]Department of Chemistry, University of California, Berkeley, Berkeley, CA, USA. [21]Gladstone Institute of Data Science and Biotechnology, Gladstone Institutes, San Francisco, CA, USA. *A list of authors and their affiliations appears at the end of the paper. ✉e-mail: pdhsu@berkeley.edu; dsavage@berkeley.edu; doudna@berkeley.edu

SARS-CoV-2 genomic RNA in human samples with PCR-derived C_t values up to 22, corresponding to ~1,600 copies per µl in the assay[21]. When tested in a mobile phone-based imaging device, this assay detects as low as ~100–200 copies per µl of target RNA within 30 min (ref. [21]). However, increased speed and sensitivity of one-pot detection chemistries are still needed to enable their widespread use for point-of-care diagnostics.

Csm6, a dimeric RNA endonuclease from type III CRISPR–Cas systems, has the potential to boost RNA detection based on its endogenous function in signal amplification[9,10,22]. During CRISPR–Cas interference, activation of Csm or Cmr by viral RNA recognition triggers synthesis of cyclic tetra- or hexaadenylates (cA_4 or cA_6) that bind to the Csm6 CRISPR-associated Rossman fold (CARF) domains and activate its higher eukaryote/prokaryote nucleotide-binding (HEPN) domains' ribonuclease activity[5,11,12,23]. However, diagnostic methods using this cascade were limited to a detection sensitivity of ~500 fM to 1 nM RNA (~10^5–10^9 copies per µl) without inclusion of RT–LAMP to amplify the target sequence[9,10]. Use of *Enterococcus italicus* Csm6 (EiCsm6) in a reaction where LwaCas13a's target-triggered *trans*-ssRNA cleavage generated linear hexaadenylates with a 2′,3′-cyclic phosphate (A_6>P, activating ligand of EiCsm6) resulted in low detection sensitivity (1 µM target RNA) and no reduction in detection time[22]. Thus, current methods using Csm6 have not resulted in a level of signal amplification that enables CRISPR proteins to directly detect RNA at a concentration relevant for diagnostics.

Here, we describe a tandem nuclease assay using Cas13a and Csm6 to achieve both high sensitivity and fast signal generation without requiring a preceding target amplification step. This involved the design of potent, chemically stabilized activators for Csm6 as well as use of eight different CRISPR RNA (crRNA) sequences for Cas13a detection. We also show that this assay can be implemented in a portable device, consisting of a microfluidic chip and a compact detector, to detect viral RNA extracted from human samples. This indicates that the assay is robust and simple to adapt for use in point-of-care testing workflows. This also highlights the value of combining unrelated CRISPR–Cas effectors for sensitive, one-pot detection of RNA.

Results

Integrating LbuCas13a and *Thermus thermophilus* Csm6 (TtCsm6) for rapid RNA detection. The minimal signal generation observed with Csm6 in RNA detection assays has limited its use for diagnostics[22]. We hypothesized that this limitation could be explained by the ability of some Csm6 proteins to degrade cA_6 or cA_4 activators over time, causing autoinactivation[23–27]. Using the Csm6 protein from the *T. thermophilus* type III-A system [12,28,29], which recognizes cA_4 or A_4>P for activation[11,12], we first tested whether 5′-$A_{3–6}U_6$-3′ oligonucleotides would produce TtCsm6-activating ligands when cleaved by RNA target-bound LbuCas13a (Fig. 1a,b). The oligonucleotide A_4-U_6 stimulated robust reporter cleavage by TtCsm6 relative to oligonucleotides containing A_3, A_5 or A_6 at the 5′ end (Fig. 1b), consistent with TtCsm6's preference for a linear activator resembling its natural cA_4 ligand[11,12]. Furthermore, the reaction requires the LbuCas13a–crRNA complex, its target RNA and the A_4-U_6 oligonucleotide, confirming that TtCsm6 activation is tightly coupled to target RNA detection by LbuCas13a via A_4-U_6 cleavage (Fig. 1c).

Activation of TtCsm6 with varying concentrations of A_4-U_6 produced an initial burst of fluorescence followed by a plateau within ~20–30 min, with the final fluorescence level proportional to the amount of Csm6 activator present (Fig. 1d). Because equal amounts of reporter molecules were present in all reactions, the plateau in the fluorescence signal likely corresponds to a cessation of reporter cleavage by TtCsm6. Addition of A_4-U_6 activator to an LbuCas13a–TtCsm6 reaction in which the fluorescence had

plateaued was shown to rapidly increase reporter cleavage by TtCsm6, while addition of more target RNA or TtCsm6 had no effect relative to a buffer control (Fig. 1e). Taken together, these data suggest that Csm6's A_4>P ligand is depleted over time, thereby deactivating its RNase activity. Consistent with this conclusion, direct activation of Csm6 with 0.5–2 µM A_4>P in the absence of LbuCas13a exhibited a similar pattern of inactivation as that observed for the full LbuCas13a–TtCsm6 reaction with A_4-U_6 (Extended Data Fig. 1a). Liquid chromatography–mass spectrometry (LC–MS) analysis also showed that A_4>P is degraded to A_2>P following incubation with TtCsm6, suggesting that linear activators, as with cyclic oligoadenylates[24–26], are subject to Csm6-catalyzed cleavage (Supplementary Table 1). In the context of the natural cA_4 ligand, A_4>P may represent an intermediate on the pathway to full TtCsm6 inactivation (Fig. 2a)[25,26].

Site-selective chemical stabilization of Csm6 activators. Mathematical modeling suggested that blocking degradation of A_4>P by Csm6 could dramatically improve fluorescent signal generation in a Cas13–Csm6 detection assay (Extended Data Fig. 2). Mutations in Csm6 or complete replacement of the 2′-hydroxyl (2′-OH) groups in cyclic oligoadenylates with 2′-fluoro (2′-F) or 2′-deoxy (2′-H) groups were previously shown to block activator degradation, but these strategies either abolished or drastically lowered the activation of Csm6 for RNA cleavage[23,25]. We wondered whether site-selective chemical modifications in linear A_4>P activators might prevent degradation of the Csm6-activating oligonucleotide, while still maintaining high-level activation of Csm6. To test whether modified linear activators can increase detection sensitivity and/or speed in a LbuCas13a–TtCsm6 assay, we replaced the 2′-hydroxyls of A_4-U_6 with either a single or triple 2′-H, 2′-F or 2′-O-methyl (2′-OMe) groups to block cleavage within the A_4 sequence (Fig. 2b and Extended Data Fig. 3a–c). Although inserting multiple modifications into the activators led to slow activation of TtCsm6, a single substitution of the 2′-hydroxyl at A2 with either a 2′-deoxy or 2′-fluoro modification boosted the target RNA detection limit from 1.25×10^6 copies per µl (2 pM) to 1.25×10^4 copies per µl (20 fM), constituting a 100-fold increase in sensitivity over an unmodified A_4-U_6 activator (Fig. 2b and Extended Data Fig. 3a–c). In addition, these singly modified activators enabled faster distinction between the sample fluorescence signal and background signal for reactions measured with 1.25×10^6 copies per µl (2 pM; above background at ~10 min), 1.25×10^5 copies per µl (200 fM; above background at ~20 min) and 1.25×10^4 copies per µl (20 fM; above background at ~40 min) of target RNA (Fig. 2b). The single-fluoro A_4-U_6 also exhibited improved signal to background over the single-deoxy A_4-U_6, indicating its superiority in maintaining TtCsm6 activation (Fig. 2b).

To confirm that the enhanced signal amplification provided by the singly modified A_4-U_6 activators was indeed due to better activation by the A_4>P ligand, we showed that A_4>P oligonucleotides containing a 2′-fluoro or 2′-deoxy at the A2 nucleotide could sustain TtCsm6's activity for longer times than the unmodified A_4>P (Extended Data Fig. 1a–c). In addition, incubation of TtCsm6 with the single-fluoro A_4>P produced A_3>P, indicating that TtCsm6-catalyzed degradation of A_4>P to A_2>P was blocked by the modification but cleavage could occur at other positions (Supplementary Tables 1 and 2). Interestingly, we found that application of an analogous single-fluoro substitution strategy to EiCsm6, an ortholog that uses cA_6/A_6>P as an activating ligand[12,23], did not lead to a substantial improvement in the sensitivity or speed of an LbuCas13a–EiCsm6 RNA detection assay (Fig. 2c and Extended Data Fig. 4a,b). It is possible that the longer A_6>P activator of EiCsm6 is more susceptible to nucleolytic degradation than the shorter A_4>P activator of TtCsm6. Taken together, these results demonstrate that the single-fluoro A_4-U_6 activator of TtCsm6
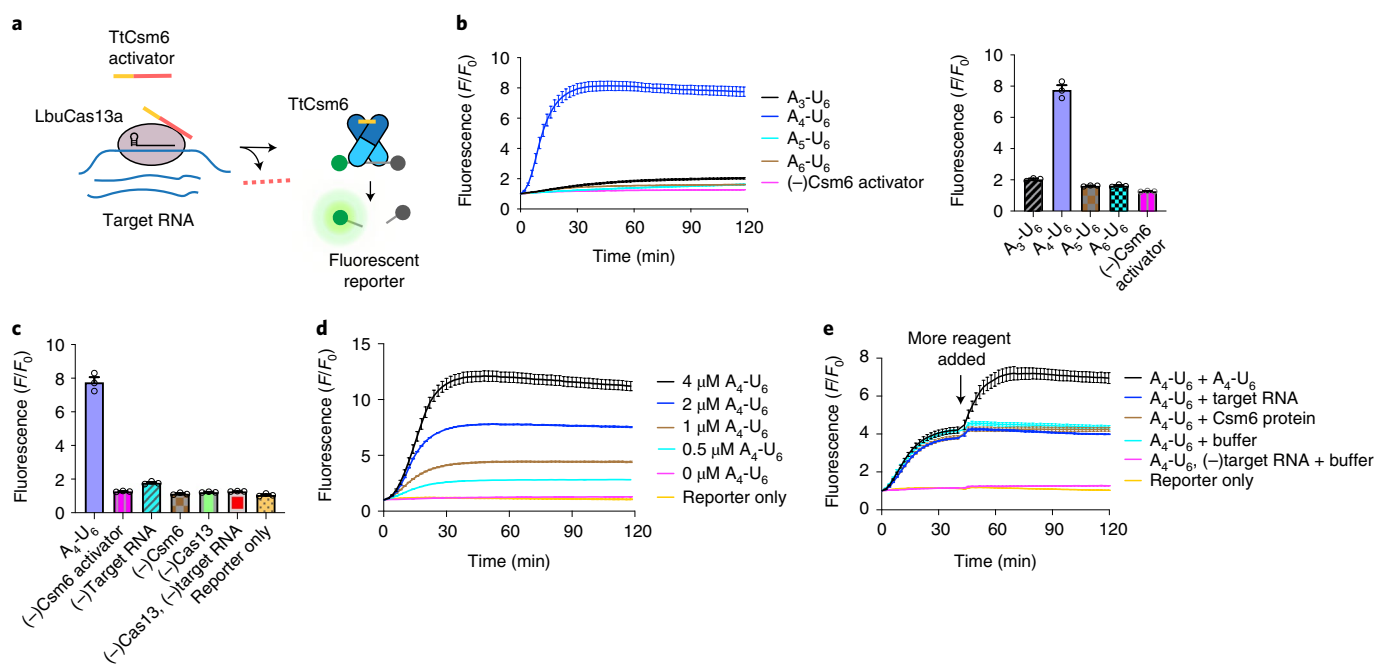
Fig. 1 | Activation and inactivation of TtCsm6 in an LbuCas13a–TtCsm6 assay. a, Schematic of TtCsm6 activation by LbuCas13a assembled with a crRNA. Binding of target RNA (blue) by LbuCas13a (pink) leads to activation of its *trans*-ssRNA cleavage, which results in trimming of the poly(U) region (red) from the TtCsm6 activator. This liberates an oligoadenylate activator with a 2′,3′-cyclic phosphate (yellow) that binds to the TtCsm6 CARF domains (dark blue) and activates the HEPN domains (light blue) for cleavage of a fluorophore quencher RNA reporter. **b**, LbuCas13a–TtCsm6 assay with TtCsm6 activators (2 μM) containing different lengths of oligoadenylates (A_3–A_6 followed by U_6). LbuCas13a is complexed with crRNA *GJK_073*, whose sequence is from a spacer found in a *Lachnospiraceae* bacterium genome. All reactions contain 200 pM target RNA (*GJK_075*). Fluorescence is plotted as F/F_0 (fluorescence (F) divided by initial fluorescence at time $t = 0$ (F_0)). The bar graph (right) shows the mean normalized fluorescence and s.e.m. as error bars ($n = 3$) at the assay endpoint (118 min). **c**, LbuCas13a–TtCsm6 assay with the A_4-U_6 oligonucleotide plotted alongside controls. Cas13 refers to LbuCas13a assembled with crRNA *GJK_073*. 'Reporter only' refers to a reaction with only the fluorescent reporter in buffer. Mean normalized fluorescence and s.e.m. ($n = 3$) at the assay endpoint of 118 min are plotted as in **b**. **d**, As in **b** but with varying concentrations of the A_4-U_6 oligonucleotide. **e**, LbuCas13a–TtCsm6 reactions with 1 μM A_4-U_6 were monitored until the signal reached a plateau. The indicated reagents (A_4-U_6 oligonucleotide, target RNA, TtCsm6 protein, or buffer) were then added to the reaction where indicated by the arrow. A control reaction without target RNA in the reaction is also overlaid for comparison (no target RNA). Mean normalized fluorescence and s.e.m. ($n = 3$) are plotted as lines with error bars.

improves signal amplification by 100-fold relative to an unmodified activator in a tandem nuclease detection assay with LbuCas13a.

Programmability and benchmarking of RNA detection. For TtCsm6 and its modified activator to be useful for enhancing RNA detection sensitivity and/or speed, the programmable nature of the CRISPR nuclease used in tandem for detection must be preserved. To test this in our Cas13–Csm6 assay, we added TtCsm6 and its single-fluoro activator to an LbuCas13a protein programmed with different crRNA sequences that target the RNA genome of SARS-CoV-2, the causative agent of COVID-19 (Fig. 3a). Detection using different crRNA sequences exhibited similar sensitivity and kinetics (Fig. 3a), showing that this one-step assay is programmable with different crRNA sequences and thus could potentially be adapted for detection of virtually any RNA sequence. To further improve detection sensitivity, we complexed LbuCas13a with a pool of eight crRNA sequences, which enables coverage of a wide range of SARS-CoV-2 variants (Supplementary Table 4) and exhibits improved signal-to-background compared to two crRNAs (Extended Data Fig. 5a–c). Using this optimized set of crRNAs, LbuCas13a could detect as few as 63 copies per μl of externally validated Biodefense and Emerging Infections (B.E.I.) SARS-CoV-2 RNA in 2 h (Fig. 3b). Inclusion of these eight guides in an LbuCas13a–TtCsm6 tandem reaction enabled detection of 31 copies per μl of SARS-CoV-2 RNA in the same time frame (Fig. 3c). To determine whether addition of TtCsm6 could accelerate the

time to detection, we compared the results of these two detection chemistries after a 20-min reaction time. While LbuCas13a was unable to detect concentrations ranging from 31 to 125 copies per μl by 20 min, the assay containing both LbuCas13a and TtCsm6 could detect 31 copies per μl within 20 min ($P < 0.05$; Fig. 3b,c and Extended Data Fig. 6). Taken together, these results demonstrate that, with optimized crRNAs for LbuCas13a and a chemically stabilized activator for TtCsm6, the tandem CRISPR nuclease assay enables amplification-free detection of RNA sequences from an infectious pathogen with both high sensitivity and a rapid time to detection.

In addition to sensitivity and speed, diagnostic assays must meet the accuracy threshold set by the Food and Drug Administration (FDA) for emergency use authorization, which stipulates that 19 of 20 replicates (95% accuracy) are detected at ~1 to 2 times the limit of detection. To determine if the LbuCas13a–TtCsm6 tandem nuclease assay would meet this validation criterion, we ran 20 replicates of our assay around the limit of detection and analyzed individual replicates by comparing them to the 95th percentile of the negative control distribution (Fig. 3d and Extended Data Figs. 7 and 8; see Methods). Our assay detected 125, 63 and 31 copies per μl of viral RNA with 100% accuracy (20/20 replicates) and 16 copies per μl with 75% accuracy (15/20 replicates) after 60 min, indicating that 31 copies per μl is the limit of detection as defined by the FDA (Fig. 3d). In addition, 125 copies per μl and 63 copies per μl of viral RNA could be detected with 95% accuracy (19/20 replicates)
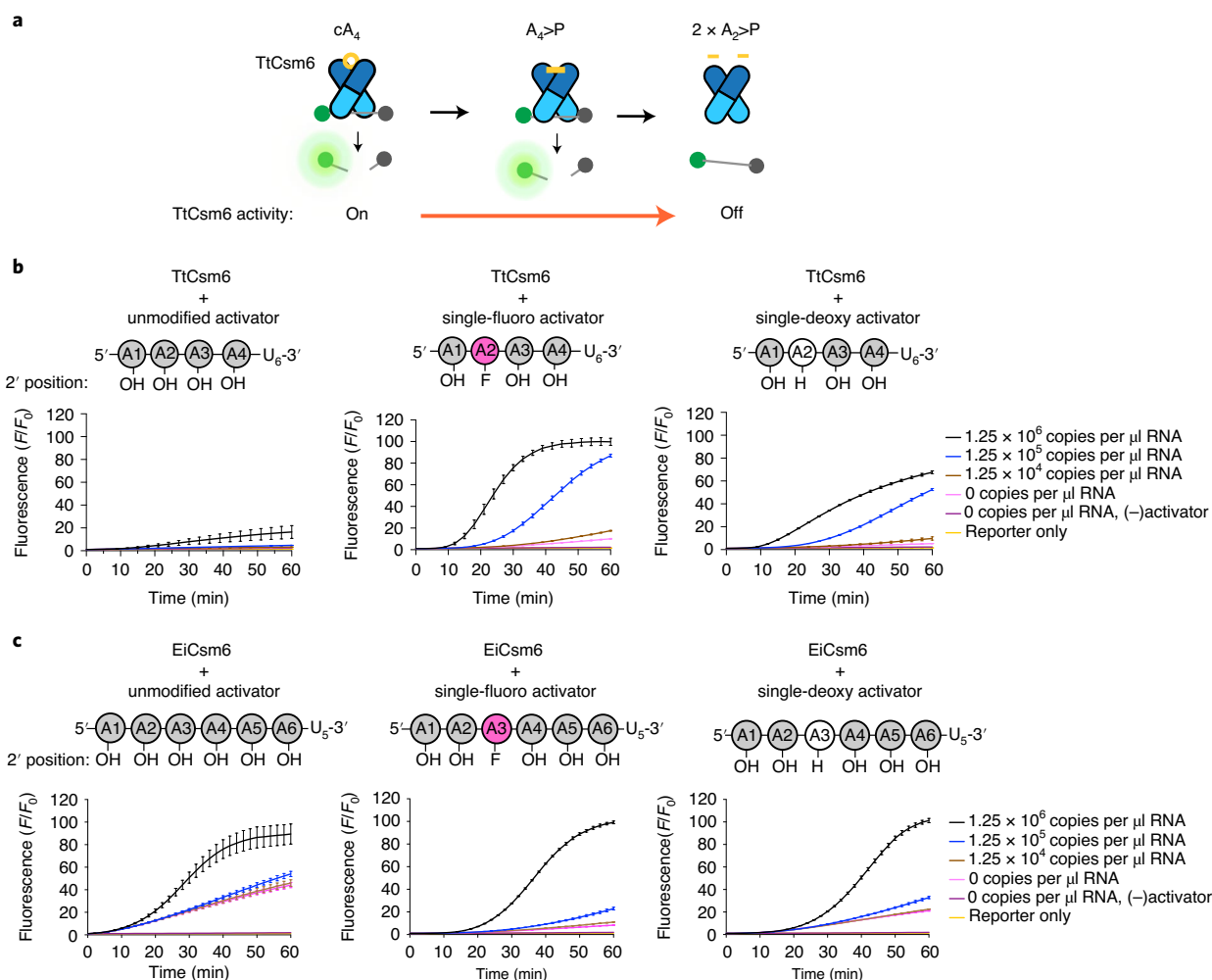
Fig. 2 | Effect of single 2′-activator modifications on Csm6-based signal generation in an RNA detection assay. a, Schematic showing degradation of cA_4 to $A_4{>}P$ and $A_2{>}P$ by TtCsm6's CARF domains (dark blue) and its effect on RNA cleavage by the HEPN domains (light blue). Binding of cA_4 or $A_4{>}P$ to TtCsm6 can activate it for ssRNA cleavage. Cleavage of cA_4 or $A_4{>}P$ to $A_2{>}P$ by the CARF domains leads to inactivation of TtCsm6's RNase activity. **b**, LbuCas13a–TtCsm6 reactions with 2 μM unmodified A_4-U_6 (left) or A_4-U_6 bearing a 2′-fluoro (F; center) or 2′-deoxy (H; right) modification on the second nucleotide (A2). LbuCas13a is assembled with crRNAs 604 and 612, which target an in vitro transcribed RNA corresponding to a fragment of the SARS-CoV-2 genome (gblock). RNA was added at concentrations ranging from 0 copies per μl to 1.25×10^6 copies per μl (2 pM). Controls lacking target RNA and the TtCsm6 activator or containing only the fluorescent reporter in buffer were run in parallel and overlaid in each panel. A schematic of the modified activator is shown above each graph. Adenosines with a 2′-hydroxyl (OH), 2′-F or 2′-H are shown in gray, pink or white, respectively. Mean normalized fluorescence and s.e.m ($n = 3$) are plotted over 60 min as lines with error bars at each measurement. **c**, As in **b**, but using EiCsm6 and its activators, which include A_6-U_5 (left), a single-fluoro A_6-U_5 (center) or a single-deoxy A_6-U_5 (right) instead of TtCsm6 and A_4-U_6 activators. The 2′ modification is on the third adenosine (A3) to block degradation of $A_6{>}P$ to $A_3{>}P$ by EiCsm6 (ref. [23]).

in 16 min and 30 min, respectively. Taken together, the performance and simplicity of the LbuCas13a–TtCsm6 tandem nuclease chemistry creates a FIND-IT assay that integrates the sensitivity of LbuCas13a with the accelerated time to detection provided by the chemically stabilized TtCsm6 activator while simultaneously achieving the accuracy required for diagnostic tests.

Detecting viral RNA with FIND-IT on a compact detector. To demonstrate the feasibility of incorporating FIND-IT into a point-of-care testing workflow, we developed a detector consisting of a microfluidic chip with reaction chambers, a heating module that maintains the reactions at 37 °C and a compact fluorescence imaging system (Fig. 4a–c). The detector, which simultaneously monitors signal from two reaction chambers, is capable of sensing changes in signal as small as 1%, corresponding to a difference of three times the root mean square error (r.m.s.e.) in

the mean signal. We applied LbuCas13a–TtCsm6 reactions containing either target RNA (B.E.I. SARS-CoV-2 genomic RNA) or water (no target RNA) to the reaction chambers and monitored the fluorescence signal for 1 h (Fig. 4d). The signal in a reaction containing 400 copies per μl of extracted SARS-CoV-2 genomic RNA increased non-linearly, resulting in a ~4.7-fold increase in 1 h, while the negative control lacking target RNA exhibited a ~1.7-fold change (Fig. 4d, left). This ~270% increase in fluorescence of the 400 copies per μl reaction compared to the background control contrasts with the ~3% variation between two negative controls run side by side (Fig. 4d, right). Given the substantial difference in output between positive and negative samples, this suggests that the LbuCas13a–TtCsm6 reaction is both chemically compatible with the microfluidic chip and, when implemented in a compact detector, could be amenable for use in point-of-care diagnostic testing strategies.
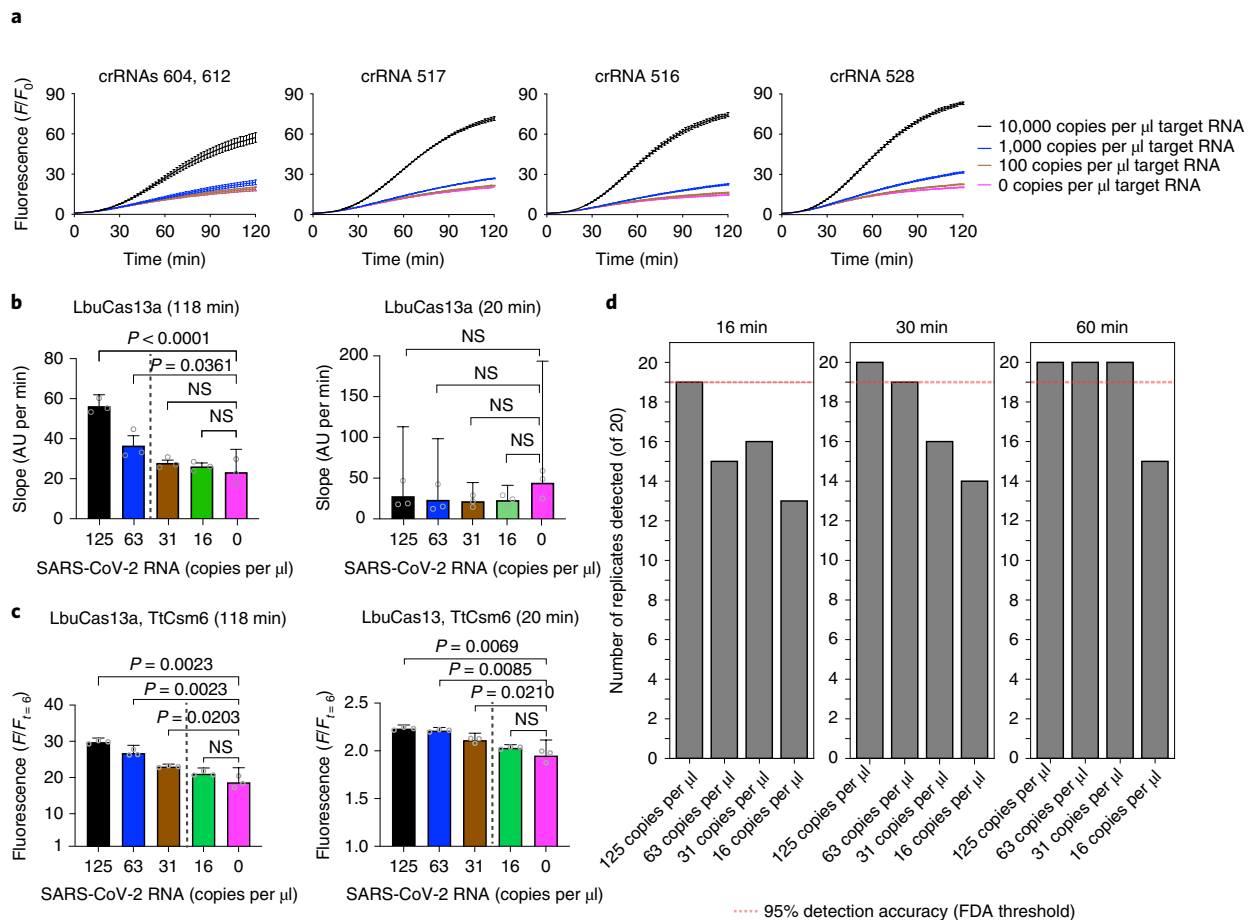
Fig. 3 | Programmability and benchmarking of the LbuCas13a–TtCsm6 assay. a, Testing the programmability of the LbuCas13a–TtCsm6 assay. LbuCas13a is assembled with crRNAs 604 and 612 (left) or other crRNAs (516, 517 or 528) targeting SARS-CoV-2 RNA. Twist synthetic SARS-CoV-2 RNA was used as the target. Mean normalized fluorescence (F/F_0) values ± s.e.m. ($n=3$) are plotted as lines with error bars over the reaction time course. **b,** Detection of B.E.I. SARS-CoV-2 RNA using LbuCas13a assembled with eight crRNAs (604, 612, 542, 546, 564, 569, 588 and 596). The slope of fluorescence increase (arbitrary units (AU) per min) due to reporter cleavage was analyzed at the assay endpoint (118 min) and at an earlier time point (20 min). The mean slope ± 95% confidence interval (CI) was plotted for each RNA concentration, with individual slopes overlaid as clear circles ($n=3$). Pairwise comparisons to the control (0 copies per μl of RNA) were done by analysis of covariance (ANCOVA), as described in ref. [21]. Two-tailed P values are shown above each individual comparison; comparisons that were not significant (NS) have a P value of >0.05 or signal that was lower than the control. RNA concentrations to the left of the dotted line were detected. **c,** LbuCas13a–TtCsm6 detection of B.E.I. SARS-CoV-2 RNA using eight crRNAs as in **b** and the single-fluoro A_4-U_6 activator of TtCsm6. The mean fluorescence ($F/F_{t=6}$) ± 95% CI was determined at 20 min and 118 min, with individual $F/F_{t=6}$ values overlaid as clear circles ($n=3$). Pairwise comparisons of reactions containing target RNA with the control (0 copies per μl of RNA) were done using an unpaired t-test with Welch's correction. One-tailed P values are shown above the graph; non-significant P values ($P>0.05$) are indicated by NS. **d,** Accuracy of the LbuCas13a–TtCsm6 assay over 20 replicates. Each replicate containing SARS-CoV-2 RNA was compared to the 95th percentile of the control distribution to determine if it had higher signal; a difference was considered significant when the P value was ≤0.05. The number detected out of 20 replicates is shown at 16, 30 and 60 min for varying concentrations of B.E.I. SARS-CoV-2 RNA. The FDA's threshold for limit of detection is shown as a red dotted line.

To test whether FIND-IT could detect SARS-CoV-2 genomic sequences in total RNA extracted from human respiratory swab samples, we tested nine positive samples with qRT–PCR-derived C_t values ranging from 9 to 33 (Supplementary Table 5) as well as six negative samples ($C_t > 37$) on the compact detector (Fig. 4e and Extended Data Fig. 9)[30]. To account for fluorescence variations from cartridge to cartridge, we determined the fluorescence change of each sample relative to a no target control that was run in parallel, as shown in Fig. 4d (Extended Data Fig. 9a,b; see Methods). To set a threshold for detection of positive signal, we required that the relative change of a sample exceed the mean and two standard deviations of the clinical negative distribution. Using this criterion, we found that FIND-IT detected nine of nine samples with C_t values ranging from 9 to 33 by 40 min, indicating concordance of our test

with the previous qRT–PCR analysis (Fig. 4e). All except one of the nine positive samples could also be detected at 20 min, highlighting the fast detection speed achievable with this tandem nuclease chemistry (Fig. 4e and Supplementary Table 5). In addition, the clinical negative samples ($C_t > 37$) were not detected above the detection threshold at 20 or 40 min (Fig. 4e). A tenfold dilution of the sample with a C_t value of 33 (~three C_t values higher; Extended Data Fig. 10) reduced signal-to-background levels, as expected (Extended Data Fig. 9a). Based on the C_t values of all COVID-19-positive samples ($n=39$) identified in samples from the IGI testing laboratory ($n=308$), our assay would be expected to detect ~95% of all positives within 40 min (Fig. 4f)[30]. This shows that, when combined with upstream RNA extraction, this assay could be used as part of a diagnostic testing workflow to capture most individuals at the early,

most infectious stages of COVID-19, when C_t values typically range between 20 and 30 (ref. [31]).

Discussion

CRISPR–Cas nucleases are attractive tools for diagnostic applications given their programmability and ability to directly detect sequences in viral genomes. However, increases in the sensitivity and speed of CRISPR-based detection are needed to enable widespread use of these technologies as diagnostics. In this study, we demonstrate that LbuCas13a can be coupled with TtCsm6 using chemically modified RNA activators, leading to a 100-fold increase in sensitivity over unmodified activators. Combining TtCsm6 with an LbuCas13a effector containing eight different crRNAs also enabled detection of as low as 31 copies per µl of extracted viral RNA, with detection accuracy reaching 100% by 60 min over 20 replicates. Higher viral RNA concentrations can be detected with similar accuracy at earlier time points, with 125 copies per µl and 63 copies per µl detected in 16 and 30 min, respectively. We also show that the intrinsic programmability of LbuCas13a is preserved in this assay with different crRNAs targeting the SARS-CoV-2 viral genome. The assay can be readily adapted to a compact device composed of a microfluidic cartridge integrated with a compact LED camera. It also detected SARS-CoV-2 RNA in clinical samples with C_t values ranging between 9 and 33, indicating its ability to potentially capture individuals at highly infectious stages of disease[31]. Full concordance of positive sample detection with previous analysis by qRT–PCR in the IGI testing lab was also observed by 40 min. Implementation of a full point-of-care testing strategy using FIND-IT will require additional development of suitable sample collection and processing procedures as well as a robust data analysis and management pipeline. Future studies with greater numbers of human samples will also be needed for clinical validation of diagnostic tests that utilize FIND-IT for RNA detection. The sensitive and accelerated response of this one-pot detection chemistry could

have broad use for detection of SARS-CoV-2 RNA and also other viral or cellular RNA sequences in the future.

This approach is one of the few diagnostic technologies that does not require target amplification, relying instead on tandem nucleases, Cas13 and Csm6, to directly sense RNA with both high sensitivity and fast signal generation. It achieves a sensitivity of 31 copies per µl of RNA, which is lower than the 100 copies per µl concentration considered to be useful for diagnostic surveillance and pandemic control[1]. Importantly, the FIND-IT chemistry can reach this detection sensitivity rapidly and in the context of a single combined reaction containing both nucleases and the activator oligonucleotide. This workflow could potentially reduce costs and simplify the development of point-of-care tests compared to assays that require additional reagents for reverse transcription, target amplification and in vitro transcription before CRISPR-based detection[9,10,16,17,20,22]. Amplification-free chemistries would also help meet a critical need when the supply of amplification-based reagents is strained, such as during a pandemic. Removing the amplification step also lowers the risk of target contamination both within and across sample batches. Finally, Csm6 has the potential to be integrated with other Cas13-based RNA detection platforms[21,32] and thus could enhance time to detection and/or sensitivity for a variety of diagnostic applications.

Fig. 4 | Implementing FIND-IT on a compact fluorescence detector for analysis of COVID-19 samples. a, A compact and sensitive fluorescence detector for the FIND-IT assay. The heating module (I), sample cartridge (II), imaging optics (III) and camera (IV) are indicated by Roman numerals. The size of the imaging optical train is shown above. **b**, Photograph showing the compact fluorescence imaging system; scale bar, 20 mm. **c**, Photograph showing the imaging chambers on the microfluidic chip; scale bar, 1.75 mm. **d**, Detection of B.E.I. SARS-CoV-2 RNA on a compact detector using the FIND-IT assay. Either 400 copies per µl of RNA or water (0 copies per µl) was added to the reactions. Images (top) show the reaction mixture in the imaging wells after 60 min, and graphs (bottom) show the full time courses of the normalized fluorescence signal (F/F_0) for each well over 1 h. Examples of regions of interest used for integrating fluorescence intensity in the wells are shown as orange boxes. **e**, Detection of SARS-CoV-2 RNA in total RNA extracted from respiratory swab samples obtained from the Innovative Genomics Institute (IGI) testing laboratory[30]. Each sample was run in parallel on the microfluidic chip with a no target control (0 copies per µl), as in **d**. Nine positive samples ($C_t = 9$ to 33) and six negative samples ($C_t > 37$) were tested, and their relative fluorescence change over background was determined. The detection threshold was set as two s.d. above the mean fluorescence change of negative samples relative to their controls ($n = 6$; see Methods). The percentage of positive and negative samples detected by 20 min (dark blue) and 40 min (light blue) is shown. Full time course data are provided in Extended Data Fig. 9, and individual C_t values of the samples are provided in Supplementary Table 5. **f**, Scatter dot plot showing the C_t values of 39 positive samples identified in a total of 308 samples obtained from the IGI testing laboratory[30]. A green dotted line indicates a C_t value of 33, corresponding to the highest C_t value detected by FIND-IT in **e**.
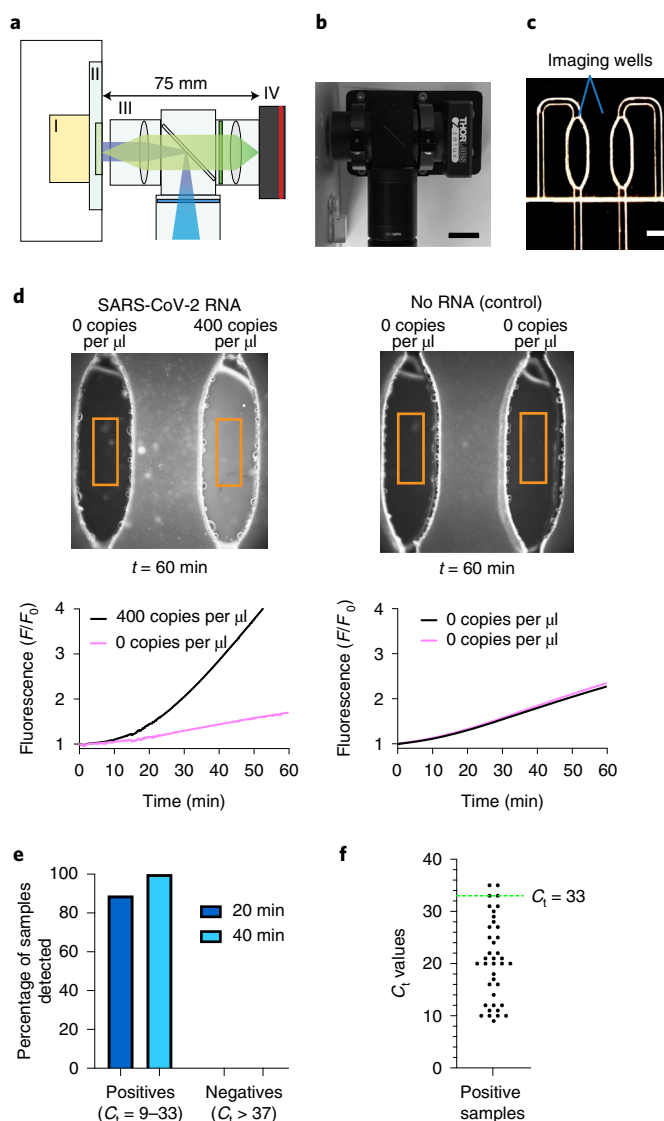
These results establish FIND-IT as a simple, one-pot assay that enables rapid RNA detection with high sensitivity and accuracy. The programmability of FIND-IT also indicates that it could be adapted to detect virtually any RNA sequence. Furthermore, we show that this assay can be implemented on a compact detector and thus would be amenable for use in point-of-care diagnostics. FIND-IT demonstrates the value of stabilizing Csm6 nuclease activation and deploying it in tandem with RNA-cleaving CRISPR–Cas proteins for fast, sensitive RNA detection in a simple, amplification-free format[33–36]. This technology could enable practical on-site detection of viral or human RNA in clinical samples or plant, fungal or microbial RNA in environmental samples.

Online content

Any methods, additional references, Nature Research reporting summaries, source data, extended data, supplementary information, acknowledgements, peer review information; details of author contributions and competing interests; and statements of data and code availability are available at https://doi.org/10.1038/s41589-021-00842-2.

References

1. Larremore, D. B. et al. Test sensitivity is secondary to frequency and turnaround time for COVID-19 screening. *Sci. Adv.* **7**, eabd5393 (2021).
2. Vogels, C. B. F. et al. Analytical sensitivity and efficiency comparisons of SARS-CoV-2 RT–qPCR primer–probe sets. *Nat. Microbiol.* **5**, 1299–1305 (2020).
3. Mina, M. J., Parker, R. & Larremore, D. B. Rethinking COVID-19 test sensitivity—a strategy for containment. *N. Engl. J. Med.* **383**, e120 (2020).
4. Knott, G. J. & Doudna, J. A. CRISPR–Cas guides the future of genetic engineering. *Science* **361**, 866–869 (2018).
5. Liu, T. Y. & Doudna, J. A. Chemistry of class 1 CRISPR–Cas effectors: binding, editing, and regulation. *J. Biol. Chem.* **295**, 14473–14487 (2020).
6. Makarova, K. S. et al. Evolutionary classification of CRISPR–Cas systems: a burst of class 2 and derived variants. *Nat. Rev. Microbiol.* **18**, 67–83 (2020).
7. East-Seletsky, A. et al. Two distinct RNase activities of CRISPR–C2c2 enable guide-RNA processing and RNA detection. *Nature* **538**, 270–273 (2016).
8. Gootenberg, J. S. et al. Nucleic acid detection with CRISPR–Cas13a/C2c2. *Science* **356**, 438–442 (2017).
9. Steens, J. A. et al. SCOPE: flexible targeting and stringent CARF activation enables type III CRISPR–Cas diagnostics. Preprint at *bioRxiv* https://doi.org/10.1101/2021.02.01.429135 (2021).
10. Santiago-Frangos, A. et al. Intrinsic signal amplification by type-III CRISPR-Cas systems provides a sequence-specific SARS-CoV-2 diagnostic. *Cell Rep. Med.* **2**, 100319 (2021).
11. Kazlauskiene, M., Kostiuk, G., Venclovas, Č., Tamulaitis, G. & Siksnys, V. A cyclic oligonucleotide signaling pathway in type III CRISPR–Cas systems. *Science* **357**, 605–609 (2017).
12. Niewoehner, O. et al. Type III CRISPR–Cas systems produce cyclic oligoadenylate second messengers. *Nature* **548**, 543–548 (2017).
13. East-Seletsky, A., O'Connell, M. R., Burstein, D., Knott, G. J. & Doudna, J. A. RNA targeting by functionally orthogonal type VI-A CRISPR–Cas enzymes. *Mol. Cell* **66**, 373–383 (2017).
14. Nagamine, K., Hase, T. & Notomi, T. Accelerated reaction by loop-mediated isothermal amplification using loop primers. *Mol. Cell. Probes* **16**, 223–229 (2002).
15. Piepenburg, O., Williams, C. H., Stemple, D. L. & Armes, N. A. DNA detection using recombination proteins. *PLoS Biol.* **4**, e204 (2006).
16. Joung, J. et al. Detection of SARS-CoV-2 with SHERLOCK one-pot testing. *N. Engl. J. Med.* **383**, 1492–1494 (2020).
17. Broughton, J. P. et al. CRISPR–Cas12-based detection of SARS-CoV-2. *Nat. Biotechnol.* **38**, 870–874 (2020).
18. Joung, J. et al. Point-of-care testing for COVID-19 using SHERLOCK diagnostics. Preprint at *medRxiv* https://doi.org/10.1101/2020.05.04.20091231 (2020).
19. Arizti-Sanz, J. et al. Streamlined inactivation, amplification, and Cas13-based detection of SARS-CoV-2. *Nat. Commun.* **11**, 5921 (2020).
20. Zhang, F., Abudayyeh, O. O., & Gootenberg, J. S. A protocol for detection of COVID-19 using CRISPR diagnostics. https://www.broadinstitute.org/files/publications/special/COVID-19%20detection%20(updated).pdf (2020).
21. Fozouni, P. et al. Amplification-free detection of SARS-CoV-2 with CRISPR–Cas13a and mobile phone microscopy. *Cell* **184**, 323–333 (2021).
22. Gootenberg, J. S. et al. Multiplexed and portable nucleic acid detection platform with Cas13, Cas12a, and Csm6. *Science* **360**, 439–444 (2018).
23. Garcia-Doval, C. et al. Activation and self-inactivation mechanisms of the cyclic oligoadenylate-dependent CRISPR ribonuclease Csm6. *Nat. Commun.* **11**, 1596 (2020).
24. Athukoralage, J. S., Rouillon, C., Graham, S., Grüschow, S. & White, M. F. Ring nucleases deactivate type III CRISPR ribonucleases by degrading cyclic oligoadenylate. *Nature* **562**, 277–280 (2018).
25. Jia, N., Jones, R., Yang, G., Ouerfelli, O. & Patel, D. J. CRISPR–Cas III-A Csm6 CARF domain is a ring nuclease triggering stepwise cA4 cleavage with ApA>p formation terminating RNase activity. *Mol. Cell* **75**, 944–956 (2019).
26. Athukoralage, J. S., Graham, S., Grüschow, S., Rouillon, C. & White, M. F. A type III CRISPR ancillary ribonuclease degrades its cyclic oligoadenylate activator. *J. Mol. Biol.* **431**, 2894–2899 (2019).
27. Smalakyte, D. et al. Type III-A CRISPR-associated protein Csm6 degrades cyclic hexa-adenylate activator using both CARF and HEPN domains. *Nucleic Acids Res.* **48**, 9204–9217 (2020).
28. Liu, T. Y., Liu, J.-J., Aditham, A. J., Nogales, E. & Doudna, J. A. Target preference of type III-A CRISPR–Cas complexes at the transcription bubble. *Nat. Commun.* **10**, 3001 (2019).
29. Niewoehner, O. & Jinek, M. Structural basis for the endoribonuclease activity of the type III-A CRISPR-associated protein Csm6. *RNA* **22**, 318–329 (2016).
30. IGI Testing Consortium. Blueprint for a pop-up SARS-CoV-2 testing lab. *Nat. Biotechnol.* **38**, 791–797 (2020).
31. Bullard, J. et al. Predicting infectious severe acute respiratory syndrome coronavirus 2 from diagnostic samples. *Clin. Infect. Dis.* **71**, 2663–2666 (2020).
32. Ackerman, C. M. et al. Massively multiplexed nucleic acid detection using Cas13. *Nature* **582**, 277–282 (2020).
33. McMahon, S. A. et al. Structure and mechanism of a type III CRISPR defence DNA nuclease activated by cyclic oligoadenylate. *Nat. Commun.* **11**, 500 (2020).
34. Lau, R. K. et al. Structure and mechanism of a cyclic trinucleotide-activated bacterial endonuclease mediating bacteriophage immunity. *Mol. Cell* **77**, 723–733 (2020).
35. Rostøl, J. T. et al. The Card1 nuclease provides defence during type III CRISPR immunity. *Nature* **590**, 624–629 (2021).
36. Molina, R. et al. Structure of Csx1–cOA4 complex reveals the basis of RNA decay in type III-B CRISPR–Cas. *Nat. Commun.* **10**, 4302 (2019).

IGI Testing Consortium

Jennifer R. Hamilton[2], Enrique Lin-Shiao[2], Elizabeth C. Stahl[2], Connor A. Tsuchida[2], Erica A. Moehle[2], Petros Giannikopoulos[2], Matthew McElroy[2], Shana McDevitt[2], Arielle Zur[2], Iman Sylvain[2], Alison Ciling[2], Madeleine Zhu[2], Clara Williams[2] and Alisha Baldwin[2]

A full list of members appears in the Supplementary Information.

Methods

Protein purification. The DNA construct encoding LbuCas13a was codon-optimized for expression in *E. coli* and cloned with an N-terminal His-SUMO tag by Genscript (pGJK_His-SUMO-LbuCas13a)[13]. LbuCas13a expression and purification were performed as previously described[13] with modifications. A construct encoding for N-terminal His$_6$-maltose binding protein (MBP)-tagged LbuCas13a (p2CT-His-MBP-Lbu_C2c2_WT; used in Fig. 1 and Extended Data Fig. 3) or His$_6$-SUMO-tagged LbuCas13a (used in Figs. 2–4 and Extended Data Figs. 1 and 4–9) was transformed into *E. coli* Rosetta 2(DE3) pLysS cells cultured in Terrific broth at 37 °C and expressed as described previously[13]. Cell pellets were resuspended in lysis buffer (50 mM HEPES, pH 7.0, 500 mM NaCl, 1 mM TCEP, 10% glycerol, 0.5 mM phenylmethylsulfonyl fluoride (PMSF) and EDTA-free protease inhibitor tablets (Roche)) and lysed by sonication. Following centrifugation, the clarified lysate of His$_6$-MBP-LbuCas13a or His$_6$-SUMO-LbuCas13a was applied to a HiTrap Ni-NTA column (GE Healthcare) and eluted over a linear imidazole (0.01–0.3 M) gradient. TEV or SUMO protease was added to remove the MBP or SUMO tag, respectively, and the protein was dialyzed overnight at 4 °C. LbuCas13a was further purified by ion exchange using a HiTrap SP column (GE Healthcare) and, in the case of the MBP-tagged construct, by an MBP trap HP column (GE Healthcare). Finally, size-exclusion chromatography (SEC) was performed using a Superdex 200 16/600 column (GE Healthcare) in buffer containing 20 mM HEPES, pH 7.0, 200 mM KCl, 10% glycerol and 1 mM TCEP. Peak fractions were pooled, concentrated and flash frozen in aliquots with liquid nitrogen.

The codon-optimized sequence encoding residues 2–467 of TtCsm6 (also known as TTHB152) was cloned into the 1S expression vector as an N-terminal His$_6$-SUMO-tagged protein with a TEV cleavage site (pET_His6-SUMO-TEV-TtCsm6). The protein was expressed in BL21(DE3) cells, as described previously[29]. Cell pellets were resuspended in lysis buffer (20 mM HEPES, pH 8.0, 500 mM KCl, 5 mM imidazole and 1 mM TCEP) supplemented with EDTA-free protease inhibitor tablets (Roche) and lysed by sonication. Following centrifugation, the clarified lysate was mixed with HIS-Select Nickel Affinity Gel (Sigma) at 4 °C, and the resin was washed with lysis buffer. The protein was eluted with 250 mM imidazole. TEV protease was added to remove the His-SUMO tag, and the protein was dialyzed overnight at 4 °C against buffer containing 25 mM HEPES, pH 7.5, 150 mM NaCl, 5% (vol/vol) glycerol and 1 mM TCEP. The protein was centrifuged to remove aggregates, concentrated and subjected to SEC on a Superdex 200 16/600 column (GE Healthcare). Peak fractions were pooled, concentrated to ~600 μM and flash frozen in liquid nitrogen. Working stocks were prepared by diluting the protein in buffer containing 20 mM HEPES, pH 7.5, 200 mM KCl, 5% (vol/vol) glycerol and 1 mM TCEP and flash freezing in small aliquots with liquid nitrogen.

The codon-optimized DNA sequence encoding EiCsm6 was synthesized and cloned into a pET expression vector encoding His$_6$-tagged EiCsm6 with a TEV cleavage site (ENLYFQG) by Genscript. EiCsm6 was expressed and purified by Shanghai ChemPartner. Briefly, the plasmid encoding His-EiCsm6 was transformed into BL21(DE3) Star cells and grown in LB broth at 37 °C to an optical density (OD) of ~0.6. Expression was induced with 0.5 mM IPTG, and cultures were transferred to 18 °C for 16 h. Cells were collected by centrifugation, and pellets were resuspended in lysis buffer (20 mM HEPES, pH 7.5, 500 mM KCl and 5 mM imidazole) supplemented with EDTA-free protease inhibitors (Roche) and lysed by sonication. The protein was immobilized on a 5-ml Ni-NTA fast-flow column, washed with lysis buffer and eluted with a step gradient of imidazole, with fractions at 16%, 50% and 100% elution buffer (20 mM HEPES, pH 7.5, 500 mM KCl and 500 mM imidazole) collected for further purification. The protein was incubated with TEV protease for 32 h at 25 °C to remove the His$_6$ tag. Then, the protein was reapplied to the Ni-NTA column and washed with 20 mM HEPES, pH 7.5, and 500 mM KCl, and untagged protein was eluted with 20 mM imidazole. The protein was further purified using SEC in buffer containing 20 mM HEPES, pH 7.5, 500 mM KCl and 5% (vol/vol) glycerol. Peak fractions were collected and concentrated to ~15 mg ml^{-1} and flash frozen in aliquots with liquid nitrogen.

Oligonucleotides. RNA reporter oligonucleotides are composed of either a pentacytosine sequence (C5) for Cas13a–Csm6 or Csm6-only assays or a pentauridine sequence (U5) for Cas13a-only assays, and are labeled with a 5′-fluorescein and 3′-Iowa Black moiety; they were ordered HPLC-purified from IDT in bulk (250 nmol to 1 μmol) to avoid batch-to-batch variation in basal fluorescence. For direct comparisons of reactions done with different activators or target concentrations, the same lot of reporter from IDT was always used. Cas13a crRNAs, *GJK_073* and *R004*, were ordered as desalted oligonucleotides from IDT (25-nmol scale), and crRNAs targeting different regions of the SARS-CoV-2 genome (516, 517, 528, 604, 612, 542, 546, 564, 569, 588 and 596) were ordered as desalted oligonucleotides from Synthego (5-nmol scale). Unmodified and 2′-modified A$_4$>P oligonucleotides were synthesized by IDT (250-nmol scale). Sequences of RNA oligonucleotides are listed in Supplementary Table 3. The set of eight crRNAs bound to LbuCas13a (604, 612, 542, 546, 564, 569, 588 and 596) in Figs. 3b–d and 4d,e are able to detect all published SARS-CoV-2 strains in silico (51,631 complete SARS-CoV-2 genome sequences were downloaded from NCBI

under the taxonomy ID 2697049 as of 4 March 2021). The inclusivity for each guide is listed in Supplementary Table 4.

Preparation and source of SARS-CoV-2 RNA targets. An in vitro transcribed RNA corresponding to a fragment of the SARS-CoV-2 genome was used as a target in Fig. 2 and Extended Data Fig. 4. A gene fragment (gBlock) corresponding to nucleotides 27,222–29,890 of the SARS-CoV-2 Wuhan-Hu-1 variant genome (MN908947.2) was PCR amplified with a 5′ primer bearing an extended T7 promoter sequence (GTCGAAA**TTAATACGACTCACTATAGG**) before separating and extracting the template on an agarose (2% wt/vol) gel (0.5× TAE buffer) and further purifying it by phenol–chloroform extraction (pH 8.0) and ethanol precipitation. The highly purified and RNase-free template was used in a high-yield in vitro transcription reaction containing 1× transcription buffer (30 mM Tris-Cl, 25 mM MgCl$_2$, 0.01% (vol/vol) Triton X-100 and 2 mM spermidine, pH 8.1), 5 mM of each NTP, 10 mM DTT, 1 μg ml^{-1} pyrophosphatase (Roche) and 100 μg ml^{-1} T7 RNA polymerase (purified in-house) incubated at 37 °C for 4 h. The reaction was quenched with the addition of 25 U of RNase-free DNase (Promega) at 37 °C for 30 min before the addition of two volumes of acidic phenol and subsequent phenol–chloroform extraction. The RNA was then ethanol-precipitated and flash frozen for storage at −80 °C. The sequence of the resulting transcript is provided in Supplementary Table 3.

Twist synthetic SARS-CoV-2 RNA control 2 (102024) was used as a target in Fig. 3a and Extended Data Fig. 5. Extracted, externally validated SARS-CoV-2 genomic RNA from B.E.I. Resources (NIAID/NIH) was used in Figs. 3b–d and 4d and Extended Data Figs. 6–8 for better comparability to previous studies (lots 70034085 and 70034826)[21]. This reagent was deposited by the Centers for Disease Control and Prevention and was obtained through B.E.I. Resources, NIAID, NIH: Genomic RNA from SARS-Related Coronavirus 2, Isolate USA-WA1/2020, NR-52285.

LbuCas13a–Csm6 plate reader assays. In Fig. 1 and Extended Data Fig. 3, LbuCas13a–TtCsm6 reactions contained 40 nM LbuCas13a, 20 nM crRNA, 100 nM TtCsm6, 100–200 pM RNA target and 200 nM C5 reporter, with either Csm6 activator or DEPC-treated water added (no activator control). The reactions were performed at 37 °C in buffer containing 20 mM HEPES (pH 6.8), 50 mM KCl, 5 mM MgCl$_2$, 100 μg ml^{-1} bovine serum albumin (BSA), 0.01% Igepal CA-630 and 2% (vol/vol) glycerol. The LbuCas13a–crRNA complex was assembled at a concentration of 1 μM LbuCas13a and 500 nM crRNA for 15 min at room temperature. Twenty-microliter plate reader assays were started by mixing 15 μl of a master mix containing the LbuCas13a–crRNA complex and TtCsm6 in buffer with 5 μl of a second master mix containing target RNA, reporter and the Csm6 activator in buffer. The protein master mix was equilibrated to room temperature for ~15–20 min before the reaction. Fluorescence measurements were made every 2 min on a Tecan Spark plate reader (λ_{ex}, 485 nm; λ_{ex}, 535 nm), and z position was optimized to a well containing 200 nM C5 reporter in buffer.

For experiments in Fig. 1e, the reaction was initiated as in Fig. 1d with 1 μM of the A$_4$-U$_6$ activator and allowed to proceed until it reached a plateau, at which point 1 μl of either 20 μM A$_4$-U$_6$, 4 nM target RNA or 2 μM TtCsm6 was added to double the amount of each reagent in the reaction. For controls, 1 μl of the reaction buffer was added instead. The assay plate was then replaced back into the plate reader to continue the assay.

In Figs. 2b and 3, LbuCas13a–TtCsm6 reactions contained 50 nM LbuCas13a, 50 nM crRNA, 100 nM TtCsm6, 1 U μl^{-1} murine RNase inhibitor (New England Biolabs), 2 μM TtCsm6 activator and 200 nM C5 reporter, with either target RNA or DEPC water added. The reaction buffer used for these assays contained 20 mM HEPES, pH 6.8, 50 mM KCl, 5 mM MgCl$_2$ and 5% (vol/vol) glycerol in DEPC-treated, nuclease-free water (Fisher Scientific or Invitrogen) supplemented with 1 U μl^{-1} murine RNase inhibitor, as previously described[21]. Reactions were started by mixing 15 μl of the protein master mix containing LbuCas13a, crRNA and TtCsm6 with 5 μl of the activator/reporter master mix containing TtCsm6 activator, target RNA and a C5 reporter. In Figs. 2b,c and 3a, measurements were taken on a Biotek plate reader at 37 °C (λ_{ex}, 485 nm; λ_{ex}, 528 nm), with a z position of 10.0 mm. In Fig. 3c,d, measurements were taken on a Tecan Spark plate reader at 37 °C (λ_{ex}, 485 nm; λ_{ex}, 535 nm), with a z position optimized to a well containing 200 nM reporter in buffer. For the 20-replicate experiments in Fig. 3d, the z position and gain settings on the Tecan Spark plate reader were closely matched between datasets (gain, 75; z position, 18,962–18,966 μm) to allow for greater consistency for comparison.

For LbuCas13a–EiCsm6 assays in Fig. 2c and Extended Data Fig. 4, the same buffer and concentrations of LbuCas13a, crRNA and reporter were used as for the LbuCas13a–TtCsm6 assays, except 10 nM EiCsm6 and 0.5 μM EiCsm6 activator were added instead of TtCsm6 and its activator. Twenty-microliter reactions were executed as described for LbuCas13a–TtCsm6 experiments on a Biotek plate reader, with measurements taken every 2 or 3 min.

All plate reader assays were performed in low-volume, flat-bottom, black 384-well plates with a non-binding surface treatment (Corning, catalog no. 3820). The experiments in Extended Data Fig. 4 used a similar plate type without a non-binding surface treatment (Corning, catalog no. 3821). Fluorescence of Csm6 reactions was normalized where indicated by dividing all values by the initial value

at $t = 0\,min$ (F/F_0) for each replicate, except in Fig. 3c,d and Extended Data Figs. 7 and 8, where they were normalized to $t = 6\,min$ ($F/F_{t=6}$) to allow for ~5 min of temperature equilibration in the plate reader at the start of the assay. Optically clear ABsolute qPCR Plate Seals (Thermo Fisher Scientific, catalog no. AB1170) were used to seal the assay plates when using B.E.I. SARS-CoV-2 genomic RNA as the target. All LbuCas13a–Csm6 plate reader experiments in Figs. 1, 2 and 3a,c and Extended Data Figs. 1, 3, 4 and 6 were performed in triplicate. Normalized fluorescence was determined by dividing each replicate by its initial value at 0 min (F/F_0) or 6 min ($F/F_{t=6}$) and then calculating the mean and s.e.m. of three replicates.

Direct activation of TtCsm6 by A$_4$>P oligonucleotides. For direct activation experiments, 100 nM TtCsm6 in reaction buffer (20 nM HEPES, pH 6.8, 50 mM KCl, 5 mM MgCl$_2$ and 5% (vol/vol) glycerol in DEPC-treated, nuclease-free water) with 1 U µl^{-1} murine RNase inhibitor was mixed with varying concentrations of an A$_4$>P oligonucleotide. Measurements were taken at 37 °C every 2 min in a Tecan Spark plate reader (λ_{ex}, 485 nm; λ_{ex}, 535 nm), with z height optimized to a well containing 200 nM reporter in buffer. All reactions were performed in triplicate.

Modeling of the Cas13–Csm6 detection reaction. A kinetic scheme of chemical reactions was created and populated with known kinetic rates and equilibrium constants. Kinetic rates were used where known; where only equilibrium constants were known, the forward rates were assumed to be 1 nM^{-1} × s^{-1}, and a reverse rate was chosen to produce the known equilibrium constant. Rates and equilibrium constants were similar to those reported in previous publications[7,12,23,37,38]. For the CARF domain, a K_m was known instead of a K_d, so the CARF domain's K_{cat} was subtracted from the reverse rate to produce an approximate K_d. The Cas13 background cleavage rate was set to the background rate observed in purified LbuCas13a preparations. This kinetic scheme was then converted into a system of ordinary differential equations modeling the rate of change in the concentration of each reaction component as a function of time and the concentrations of the components using Mathematica. A numerical solution to the system of ordinary differential equations was created with a time step of 0.001 s and a total time of 2,000 s using the Mathematica's NDSolve at different target RNA concentrations and K_{cat} values for the Csm6 CARF domain. The full kinetic scheme, system of ordinary differential equations and the starting conditions used are provided in Supplementary Note 1 in the Supplementary Information.

LbuCas13a direct detection experiments and analysis. These assays were performed and analyzed as described previously[21] with the following modifications. Either Twist synthetic SARS-CoV-2 RNA or externally validated B.E.I. SARS-CoV-2 genomic RNA was used as the target RNA. Data were collected on a Tecan Spark plate reader at 37 °C with a gain of 87 and a z position optimized to a well in the plate containing 400 nM reporter in buffer. Fluorescence was measured every 2 min for up to 2 h (λ_{ex}, 485 nm and 10- or 20-nm bandwidth; λ_{ex}, 535 nm and 20-nm bandwidth). Linear regression and pairwise comparison of slopes using ANCOVA were done using GraphPad Prism (version 9.1.2), considering replicate y values as individual data points[21]. For determination of the limit of detection at 20 min, we used the first 20 min of measurements in the assay. All assays were done in triplicate. Plots showing mean normalized fluorescence were generated using the same normalization method as for the LbuCas13a–TtCsm6 plate reader assays (F/F_0 or $F/F_{t=6}$).

Liquid chromatography–mass spectrometry analysis. The degradation of cA$_4$, A$_4$>P or single-fluoro A$_4$>P was examined by incubating 5 µM TtCsm6 with 25 µM activator at 37 °C for 30 min in a total volume of 15 µl. The reaction was quenched by adding 1 µl of 0.5 M EDTA and heated at 95 °C for 5 min. Samples were centrifuged to remove any aggregated TtCsm6 protein. Oligonucleotide samples were then analyzed using a Synapt G2-Si mass spectrometer that was equipped with an electrospray ionization (ESI) source and a BEH C18 ionKey (length, 50 mm; inner diameter, 150 µm; particle size, 1.7 µm; pore size, 130 Å) and connected in line with an Acquity M-class ultra-performance liquid chromatography system (UPLC; Waters). Acetonitrile, formic acid (Fisher Optima grade, 99.9%) and water purified to a resistivity of 18.2 MΩ·cm (at 25 °C) using a Milli-Q Gradient ultrapure water purification system (Millipore) were used to prepare mobile phase solvents. Solvent A was 99.9% water/0.1% formic acid, and solvent B was 99.9% acetonitrile/0.1% formic acid (vol/vol). The elution program consisted of isocratic flow at 1% B for 2 min, a linear gradient from 1% to 99% B over 2 min, isocratic flow at 99% B for 5 min, a linear gradient from 99% to 1% B over 2 min and isocratic flow at 1% B for 19 min at a flow rate of 1.5 µl min^{-1}. Mass spectra were acquired in the negative ion mode and continuum format, operating the time-of-flight mass analyzer in resolution mode, with a scan time of 1 s, over the range of mass-to-charge ratios (m/z) from 100 to 5,000. MS data acquisition and processing were performed using MassLynx software (version 4.1, Waters).

Limit of detection analysis for triplicate LbuCas13a–TtCsm6 experiments. For determination of the limit of detection using the LbuCas13a–TtCsm6 assay data in Fig. 3c, an unpaired t-test with Welch's correction was used to compare mean fluorescence ($F/F_{t=6}$, fluorescence divided by fluorescence measurement at

$t = 6\,min$) of three replicates to that of the control replicates without target RNA using GraphPad Prism (version 9.1.2). The limit of detection was determined using the triplicate data collected at 20 min and 118 min as time points for direct comparison to LbuCas13a detection assays. Comparisons with $P \leq 0.05$ were considered significant. A one-tailed P value is shown because any values lower than the no-target control were not considered significant.

Limit of detection analysis for 20-replicate LbuCas13a-TtCsm6 experiments. For all 20-replicate experiments, samples were analyzed in batches of 10, because five experimental samples and five negative controls (0 copies per µl of RNA) were started simultaneously using a multichannel pipette. Reactions were set up as described above. Data for individual replicates were normalized by dividing fluorescence measurements by the fluorescence value at $t = 6\,min$. Analysis was performed using Python (version 3.8.1) at the 16-, 30- and 60-min time points. At each time point, the mean and standard deviation of the negative controls within each batch were determined and used to fit a normal distribution. The distribution of negative control results was then used to calculate the probability of seeing a point equal to or greater than each experimental sample using the survival function of the normal distribution. This value is equivalent to a one-tailed P value associated with a null hypothesis in which the experimental value is not greater than the value of the negative control. The results show the number of experimental samples of 20 replicates that could be distinguished from the negative control distribution using a P value cutoff of 0.05. These cutoffs represent a predicted 5% false-positive rate. We did not perform multiple hypothesis correction on this analysis to mirror the analysis that would be performed in a clinical setting, where an individual's sample would not be corrected based on the number of samples run, but where type 1 error (false-positive rate) would instead be controlled by setting an appropriate P value cutoff. The full time-course data used in this analysis are in Extended Data Fig. 7, and the improved signal to noise from normalization at $t = 6\,min$ is shown in Extended Data Fig. 8.

Experiments using the compact fluorescence detector. Premixed 60-µl reactions of the FIND-IT assay were loaded directly into inlets leading to the ~15-µl imaging chambers of a microfluidic chip using a pipette until the chambers and surrounding tubing were completely filled. The custom chips were fabricated from poly(methyl methacrylate) and pressure-sensitive adhesive. Reactions were assembled using the same conditions and reagent concentrations as the reactions in Fig. 3c,d, except a total reaction volume of 60 µl was used. The RNA sample constituted 10% of the total reaction volume in all reactions with extracted RNA from clinical samples or extracted B.E.I. SARS-CoV-2 genomic RNA. For control reactions, water was added instead of target RNA. The reaction chamber temperature was maintained at 37 °C with ~1–2 °C variation between runs. Reactions were imaged every 10 s for 30–60 min using the system camera gain of 2 dB and exposure setting of 150 ms or 100 ms. Light-emitting diode (LED) excitation was strobed in synchrony with the camera exposure to avoid photobleaching between data points. For imaging the ~15-µl sample chambers, we require a fairly large field of view (FOV) and a modest numerical aperture (NA), enabling a large depth of focus without images of adjacent sample wells overlapping. To accomplish this in a relatively low-cost, compact device, we designed a custom system using a pair of eyepieces (Edmund Optics, 66-208 and 66-210), yielding a system with an NA of 0.09, a FOV diameter of 12.0 mm and a magnification of 0.54 (chosen to match the sensor size of the Thorlabs CS165MU1 camera to the FOV; sampling at ≥Nyquist is unnecessary in this 'light-bucket' application). The overall system is compact, with a nominal track length (sample to camera) of ~75 mm (Fig. 4a,b). Fluorescence filters were from Chroma Technologies (ET470/40x, T495lpxr and ET535/70m), with excitation provided by a 965-mW, 470-nm LED (Thorlabs M470L4), providing a maximum of ~225 mW into the 12-mm-diameter sample FOV in an epi-illumination Kohler geometry. Custom control of the imaging hardware was implemented in MATLAB (2020a), using Thorlabs drivers and SDK (ThorCam) to control the camera acquisition and serial communication to an Arduino Bluefruit Feather board to electronically trigger the LED illumination.

To accurately compare signals between two sample chambers, we used a prospective correction method to account for non-uniform illumination and background effects[39]. Briefly, the measured pixel intensity of reaction chambers $I_{meas}(x)$ is related to actual signal $I_{real}(x)$ through

$$I_{meas}(x) = S(x) \times (B(x) + I_{real}(x)) \qquad (1)$$

Here, S is a linear scaling factor that models distortions to an image due to illumination non-uniformity, and B is an illumination-dependent background signal that accounts for scattering and background fluorescence from the reaction chambers. Before actual measurements, we determined S and B by acquiring images of blank reaction chambers filled with 1× reaction buffer (20 mM HEPES, pH 6.8, 50 mM KCl, 5 mM MgCl$_2$ and 5% (vol/vol) glycerol in DEPC-treated, nuclease-free water) and a fluorescent slide, respectively. Experimental images were processed according to equation (1) to retrieve actual signals from each channel.

The tone, brightness and contrast of two images shown in Fig. 4d were adjusted across the entire image using Adobe Photoshop 2021 (version 22.1.1). Unprocessed images are provided in the Source Data for Fig. 4.

Detection of positive signal in clinical samples. First, illumination-corrected fluorescence values were divided by their initial measurement (F/F_0) so that the clinical sample and background control curves (no target RNA added) start at the same value. Then, the normalized fluorescence of the clinical sample was divided by the normalized fluorescence of the paired background control at 20- and 40-min time points of the assay. This is referred to as the 'relative fluorescence change' of a sample compared to its corresponding control. This analysis was performed for every positive and negative clinical sample from the IGI testing lab that was run on the detector. Then, to determine the threshold for detection, we determined the mean and standard deviation of the relative fluorescence change for the negative clinical samples ($n = 6$). We considered positive signal in a reaction as being over two standard deviations higher than the mean of the negative samples. This corresponds to signal higher than ~97.5% of the negative clinical sample distribution.

Determination of C_t values for clinical samples. Human respiratory swab specimens, including mid-turbinate (MT) nasal, oropharyngeal (OP), nasopharyngeal (NP), and combined MT/OP swabs, were collected, processed and subjected to RNA extraction and qRT–PCR using primers for SARS-CoV-2 in the IGI testing laboratory, as described previously[30]. Briefly, sample C_t values were determined using primers for the nucleocapsid protein (*N*) gene, spike protein (*S*) gene and open reading frame 1ab (*ORF1ab*) locus of SARS-CoV-2 and for MS2 phage RNA (extraction process control)[30]. The average C_t value of the SARS-CoV-2 targets for each sample was determined, rounded to the nearest whole number, and plotted in Fig. 4f. All positive samples, with C_t values plotted in Fig. 4f, originated from combined MT/OP samples. The individual C_t values for all positive samples tested are provided in the Source Data file for Fig. 4.

Determination of a standard curve for C_t values using known concentrations of RNA. Twofold dilutions of TaqPath COVID-19 Combo Kit positive control (Thermo Fisher Scientific) were made in nuclease-free water to generate indicated RNA concentrations. Five microliters of the diluted positive control was added to the multiplexed COVID-19 real-time PCR assay (Thermo Fisher Scientific), with a final reaction volume of 12.5 μl. Samples were amplified on a QuantStudio 6 per the manufacturer's protocol and analyzed using the QuantStudio 6 Design and Analysis software, version 4.2.3 (Thermo Fisher Scientific).

Reporting Summary. Further information on research design is available in the Nature Research Reporting Summary linked to this article.

Data availability
The plasmid used to express MBP-tagged LbuCas13a (p2CT-His-MBP-Lbu_C2c2_WT) is available from Addgene (83482). Plasmids used for expression of SUMO-tagged LbuCas13a (pGJK_His-SUMO-LbuCas13a), His-tagged EiCsm6 (pET28a_His-TEV-EiCsm6) and His-SUMO-tagged TtCsm6 (pET_His6-SUMO-TEV-TtCsm6) will be available from Addgene (172488, 172487 and 172486). Sequences of RNA oligonucleotides are provided in Supplementary Table 3. Source data are provided with this paper.

Code availability
All custom data analysis for the limit of detection analysis for 20-replicate FIND-IT experiments and the code used for mathematical modeling of the Cas13–Csm6 reaction and illumination correction of images are available at https://github.com/jackdesmarais/FIND-IT. An archived version is available at https://doi.org/10.5281/zenodo.4921924 (ref. [40]).

References
37. Athukoralage, J. S. et al. The dynamic interplay of host and viral enzymes in type III CRISPR-mediated cyclic nucleotide signalling. *eLife* **9**, e55852 (2020).
38. Zhou, T. et al. CRISPR/Cas13a powered portable electrochemiluminescence chip for ultrasensitive and specific miRNA detection. *Adv. Sci.* **7**, 1903661 (2020).
39. Smith, K. et al. CIDRE: an illumination-correction method for optical microscopy. *Nat. Methods* **12**, 404–406 (2015).
40. Desmarais, J. J. & Bhuiya, A. jackdesmarais/FIND-IT-paper: v1.0 (Version paper_code). *Zenodo* https://doi.org/10.5281/zenodo.4921924 (2021).

Author contributions
T.Y.L., J.A.D. and G.J.K. conceived the study. G.J.K, D.C.J.S. and T.Y.L. expressed and purified proteins. T.Y.L. and D.C.J.S. performed all biochemical experiments. T.Y.L., G.J.K., D.C.J.S., E.J.C., B.W.T., S.J., N.P. and S.A. performed initial experiments optimizing biochemical assays. T.Y.L. designed Csm6 activators with help from G.J.K. and N.P. G.J.K. prepared in vitro transcribed gBlock targets. J.J.D. analyzed the 20-replicate experiments and did modeling of the Cas13–Csm6 reaction. S.S., A.B., M.D.d.L.D., N.A.S., M.A., A.R.H., A.M.E. and R.M. developed the compact detector, data normalization method and software, with M.X.T. and D.A.F. providing supervision. T.Y.L., S.S. and J.J.D performed the statistical analysis for detection of clinical positives using FIND-IT. P.F., J.S., S.I.S., C.Z., A.M., G.J.K. and D.C.J.S. identified and analyzed crRNA sequences targeting SARS-CoV-2, with G.R.K., M.O., K.S.P. and L.F.L. providing supervision. A.T.I. performed MS data collection and analysis. S.K. and E.J.D. provided general experimental support. Authors from the IGI Testing Consortium (listed at the end of this paper) established, supervised and carried out qRT-PCR testing of clinical samples, interpreted the resulting C_t data, and provided deidentified clinical samples for FIND-IT testing. J.R.H. from the IGI Testing Consortium also performed experiments converting PCR-derived C_t values to copies of RNA per μl. T.Y.L. wrote the draft of the manuscript with assistance from G.J.K. and J.A.D. All authors edited and approved the manuscript. D.F.S., P.D.H. and J.A.D. obtained funding with significant help from N.P. Overall supervision of the project was provided by T.Y.L., G.J.K., P.D.H., D.F.S. and J.A.D.

Competing interests
D.F.S. is a cofounder of Scribe Therapeutics and a scientific advisory board member of Scribe Therapeutics and Mammoth Biosciences. P.D.H. is a cofounder of Spotlight Therapeutics and Moment Biosciences and serves on the board of directors and scientific advisory board and is a scientific advisory board member to Vial Health and Serotiny. The Regents of the University of California have patents issued and/or pending for CRISPR technologies on which J.A.D., T.Y.L., P.D.H., N.P, D.F.S., D.C.J.S., S.K., B.W.T., E.J.C., S.J. and G.J.K. are inventors. M.O., P.F., G.R.K., D.A.F., S.S. and N.A.S. have also filed patent applications related to this work. J.A.D. is a cofounder of Caribou Biosciences, Editas Medicine, Scribe Therapeutics, Intellia Therapeutics and Mammoth Biosciences. J.A.D. is a scientific advisory board member of Caribou Biosciences, Intellia Therapeutics, eFFECTOR Therapeutics, Scribe Therapeutics, Mammoth Biosciences, Synthego, Algen Biotechnologies, Felix Biosciences and Inari. J.A.D. is a Director at Johnson & Johnson and has research projects sponsored by Biogen, Pfizer, AppleTree Partners and Roche.
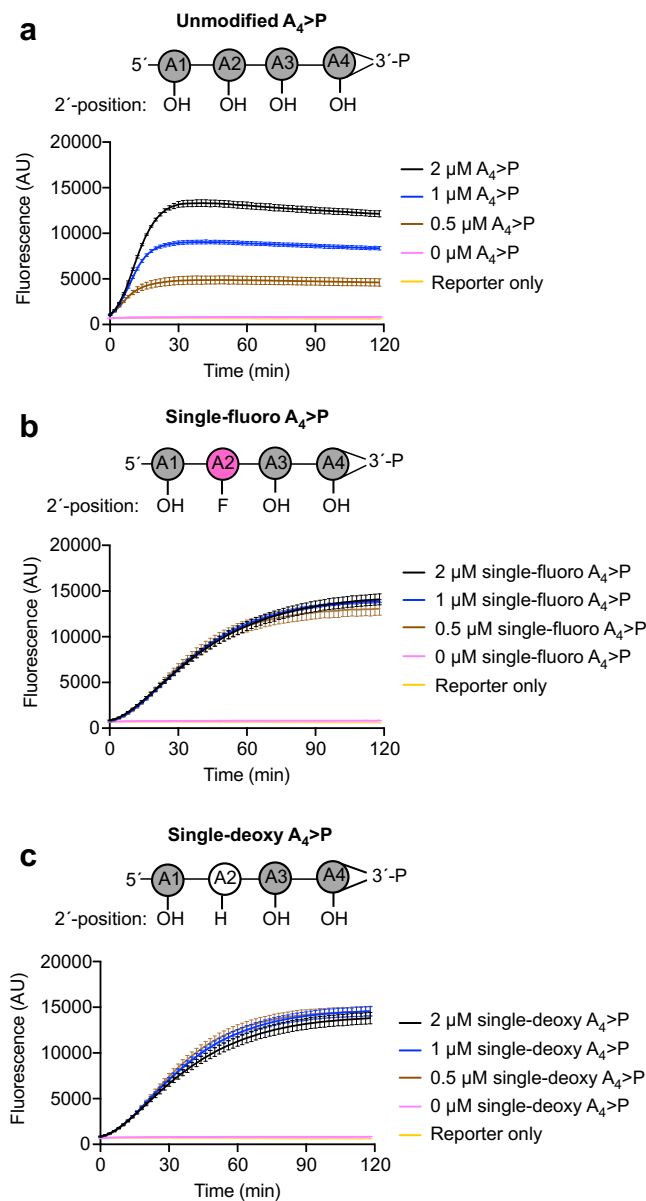
Additional information
Extended data is available for this paper at https://doi.org/10.1038/s41589-021-00842-2.

Supplementary information The online version contains supplementary material available at https://doi.org/10.1038/s41589-021-00842-2.

Correspondence and requests for materials should be addressed to P.D.H., D.F.S. or J.A.D.

Peer review information *Nature Chemical Biology* thanks Catherine Freije and the other, anonymous, reviewer(s) for their contribution to the peer review of this work.

**Reprints and permissions information** is available at www.nature.com/reprints.

a

Unmodified A$_4$>P

5′ (A1)—(A2)—(A3)—(A4) 3′-P

2′-position: OH OH OH OH

- 2 μM A$_4$>P
- 1 μM A$_4$>P
- 0.5 μM A$_4$>P
- 0 μM A$_4$>P
- Reporter only

b

Single-fluoro A$_4$>P

5′ (A1)—(A2)—(A3)—(A4) 3′-P

2′-position: OH F OH OH

- 2 μM single-fluoro A$_4$>P
- 1 μM single-fluoro A$_4$>P
- 0.5 μM single-fluoro A$_4$>P
- 0 μM single-fluoro A$_4$>P
- Reporter only

c

Single-deoxy A$_4$>P

5′ (A1)—(A2)—(A3)—(A4) 3′-P

2′-position: OH H OH OH

- 2 μM single-deoxy A$_4$>P
- 1 μM single-deoxy A$_4$>P
- 0.5 μM single-deoxy A$_4$>P
- 0 μM single-deoxy A$_4$>P
- Reporter only

Extended Data Fig. 1 | Direct activation of TtCsm6 by A$_4$>P oligonucleotides, related to Fig. 1 and Fig. 2. Direct activation of TtCsm6 with varying concentrations of the A$_4$>P oligonucleotide (tetraadenylate with 2′,3′-cyclic phosphate). Mean fluorescence intensity with error bars indicating s.e.m. (n = 3) is shown in arbitrary fluorescence units (AU). The schematic above the graph is a representation of A$_4$>P, with adenosines numbered A1-A4 from 5′ to 3′. Controls lacking TtCsm6 activator (0 μM A$_4$>P) and containing only the fluorescent reporter (Reporter only) are shown for comparison. **b)** As in **a**, but with a single-fluoro A$_4$>P oligonucleotide. The nucleotide bearing the 2′-F modification is colored pink in the schematic above the graph. **c)** As in **a**, but with a single deoxy A$_4$>P oligonucleotide. The nucleotide bearing the 2′-H modification is colored white in the schematic above the graph. Controls shown in **a** are overlaid in **b** and **c** since all experiments in this figure were run in parallel.

a Csm6 activator degradation "on"

b Csm6 activator degradation "off"
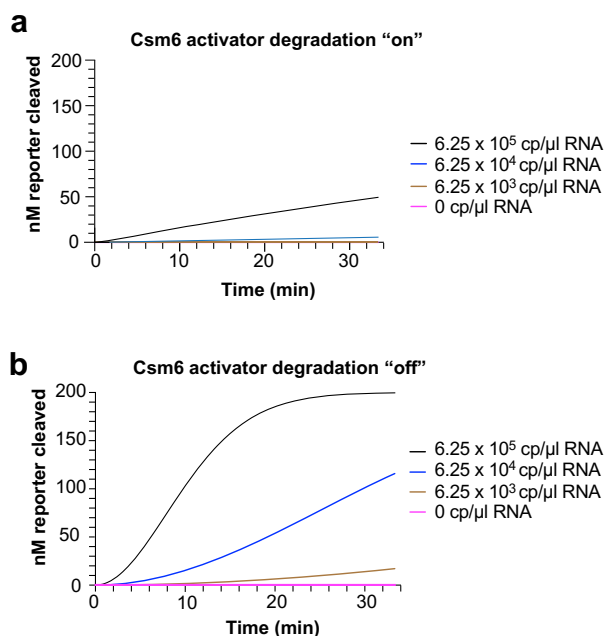
Extended Data Fig. 2 | Modeling of the Cas13-Csm6 detection reaction in the presence and absence of Csm6 activator degradation, related to Fig. 2. a) A graph showing the modeled kinetics of fluorescent reporter cleavage by the HEPN domain of Csm6 when 0 copies per µl (cp/µl) to 6.25×10^5 cp/µl (1 pM) of target RNA are present and the CARF domain is active for cleavage of $A_4{>}P$ in a Cas13-Csm6 reaction (Csm6 CARF $k_{cat} = 0.05$). $A_4{>}P$ is generated by Cas13-mediated cleavage of an A_4-U_6 oligonucleotide in the modeled reaction. **b)** As in **a**, but for a Cas13-Csm6 reaction in which the CARF domain of Csm6 is inactive for $A_4{>}P$ degradation (Csm6 CARF $k_{cat} = 0$). In this condition, the HEPN domains of $A_4{>}P$-bound Csm6 remain active for RNA cleavage over a longer time.

a

Triple-fluoro activator

b

**Triple-deoxy activator**

c

Triple-O-methyl activator
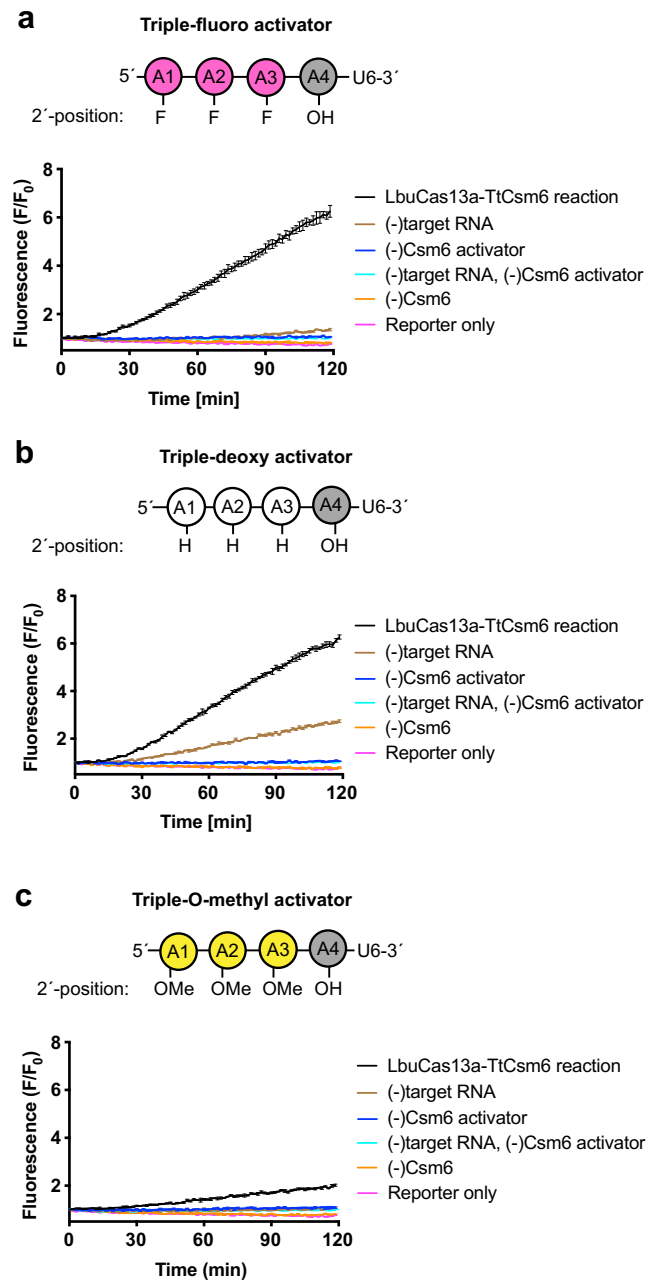
Extended Data Fig. 3 | Triple-modified TtCsm6 activators lead to slow kinetics of fluorescent signal increase in a LbuCas13a-TtCsm6 detection assay.
**a)** LbuCas13a-TtCsm6 reaction with crRNA *R004*, 100 pM of a complementary target RNA (*R010*), and 4 μM of the triple-fluoro A_4-U_6 oligonucleotide. Controls without target RNA, TtCsm6 activator, and TtCsm6 are shown, as well as a reaction with only the fluorescent reporter in buffer (Reporter only). A schematic of the activator is shown above the graph, with 2´-F nucleotides colored pink. Mean normalized fluorescence values (F/F_0) and s.e.m. (n = 3) are plotted as lines with error bars over the time course of the assay. **b)** As in **a** but with 4 μM of the triple-deoxy A_4-U_6 oligonucleotide. A schematic of the activator is shown above the graph with 2´-H nucleotides colored white. **c)** As in **a** but with 4 μM triple-O-methyl A_4-U_6 oligonucleotide. A schematic of the activator is shown above the graph with 2´-OMe nucleotides colored yellow. Controls in **a** that lack both the TtCsm6 activator and target RNA, or that contain only reporter are overlaid in **b** and **c**, as all experiments in this figure were run in parallel.

a

EiCsm6
+
Unmodified activator
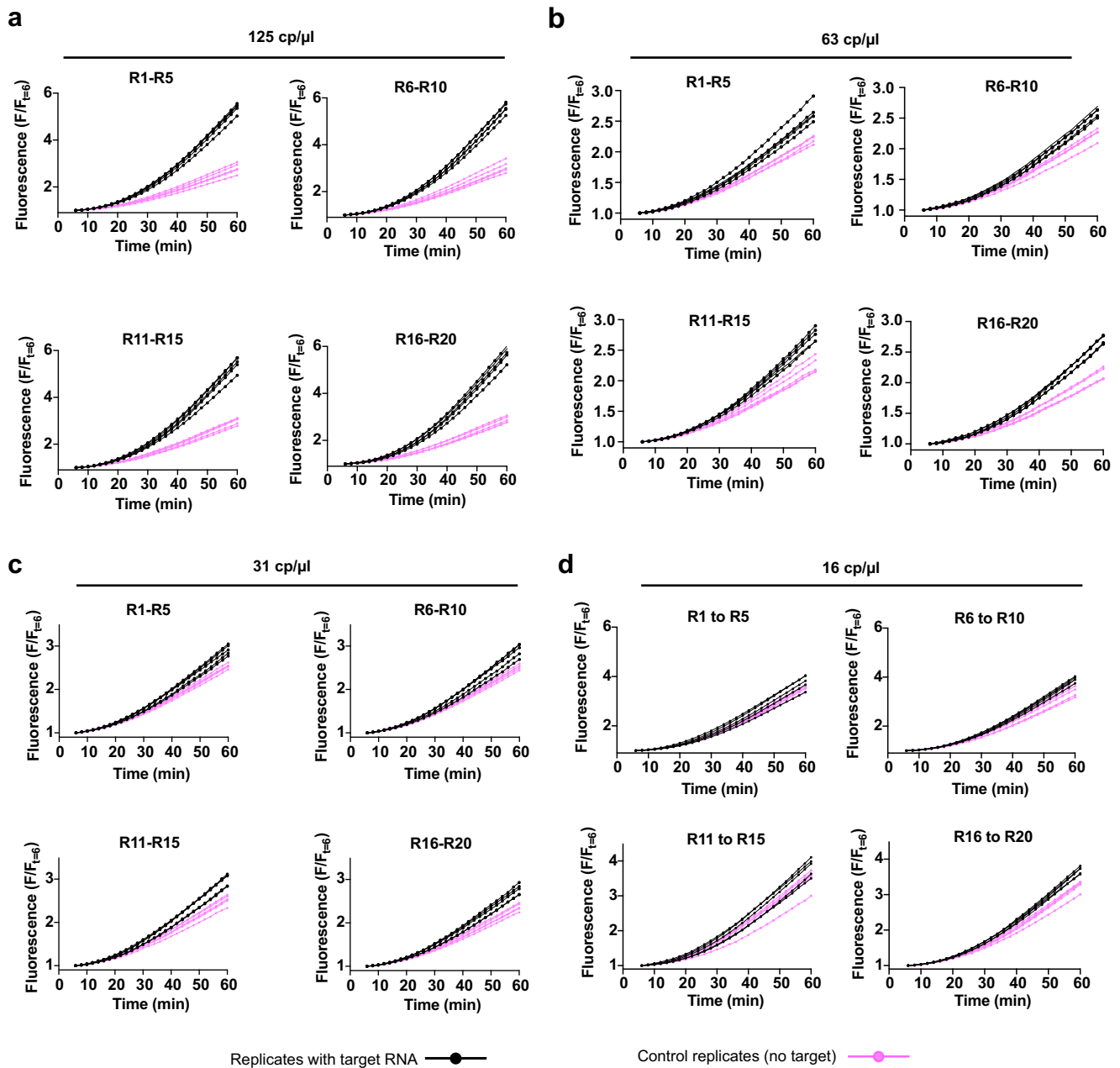

b

EiCsm6
+
Single-fluoro activator
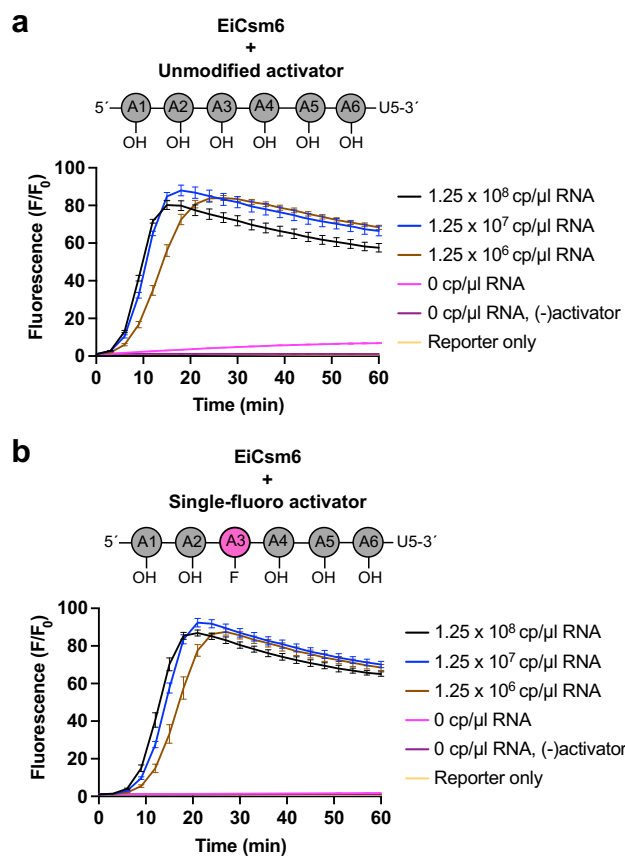
Extended Data Fig. 4 | LbuCas13a-EiCsm6 detection assay with unmodified and single-fluoro activators at high target RNA concentrations, related to Fig. 2. a) Detection assay using LbuCas13a complexed with two crRNAs, 604 and 612, and EiCsm6 with a A_6-U_5 oligonucleotide activator[22]. An *in vitro* transcribed RNA corresponding to a fragment of the SARS-CoV-2 genome (gblock) was added at concentrations ranging from 1.25×10^6 copies per µl (cp/µl) of RNA (2 pM) to 1.25×10^8 cp/µl) of RNA (200 pM). Control reactions that lack both target RNA and the EiCsm6 activator, or contain only the fluorescent reporter (Reporter only) are shown for comparison. Mean normalized fluorescence (F/F_0) and s.e.m (n = 3) are plotted as lines with error bars over the reaction time course. A schematic of the A_6-U_5 activator is shown above the graph. **b)** As in **a** but using a single-fluoro A_6-U_5 oligonucleotide as an EiCsm6 activator. The adenosine bearing a 2′-F modification is colored pink in the schematic above the graph. Controls from **a** that lack both target RNA and EiCsm6 activator, or contain only the reporter are overlaid in the graph, as all experiments in this figure were run in parallel.
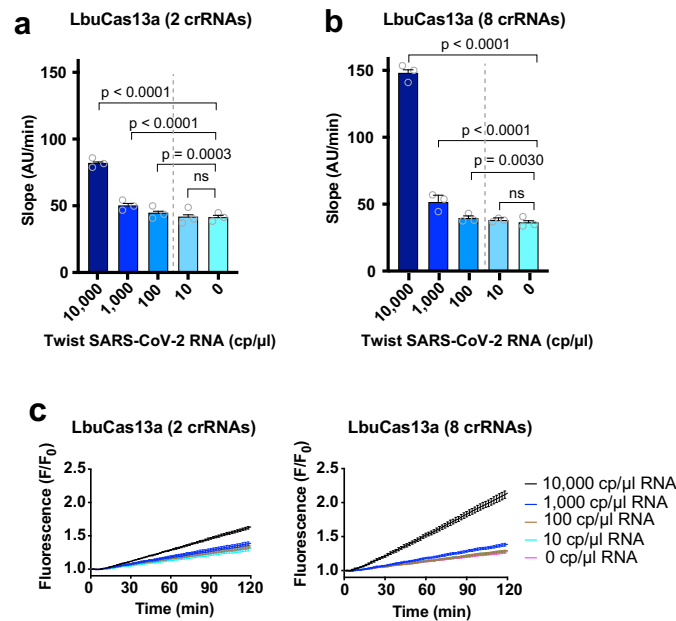
Extended Data Fig. 5 | Detection of SARS-CoV-2 RNA using LbuCas13a assembled with two or eight crRNA sequences, related to Fig. 3. a) Detection of Twist synthetic SARS-CoV-2 RNA control using LbuCas13a loaded with two different crRNAs (604 and 612). The mean slope $\pm$ 95% CI of fluorescence signal increase over 120 min was plotted, with individual slopes shown as clear circles ($n=3$). Pairwise comparisons of slopes to the control reaction with 0 copies per µl (cp/µl) of RNA was done by ANCOVA, as previously described[21]. Two-tailed P values are shown above each pairwise comparison. Non-significant P values ($P > 0.05$) are indicated with 'ns' above the comparison. Concentrations to the left of the dotted line were detected above the control. **b)** As in **a**, but with LbuCas13a complexed with eight crRNAs (604, 612, 542, 546, 564, 569, 588, 596) targeting the SARS-CoV-2 genome. **c)** Full 2-hour time course of the detection assays in **a** (left panel) and **b** (right panel), using LbuCas13a with two or eight crRNA sequences, respectively. The mean normalized fluorescence values (F/F_0) $\pm$ s.e.m. are plotted as lines with error bars over the time course. The concentration of RNA present in each reaction is shown in the legend.
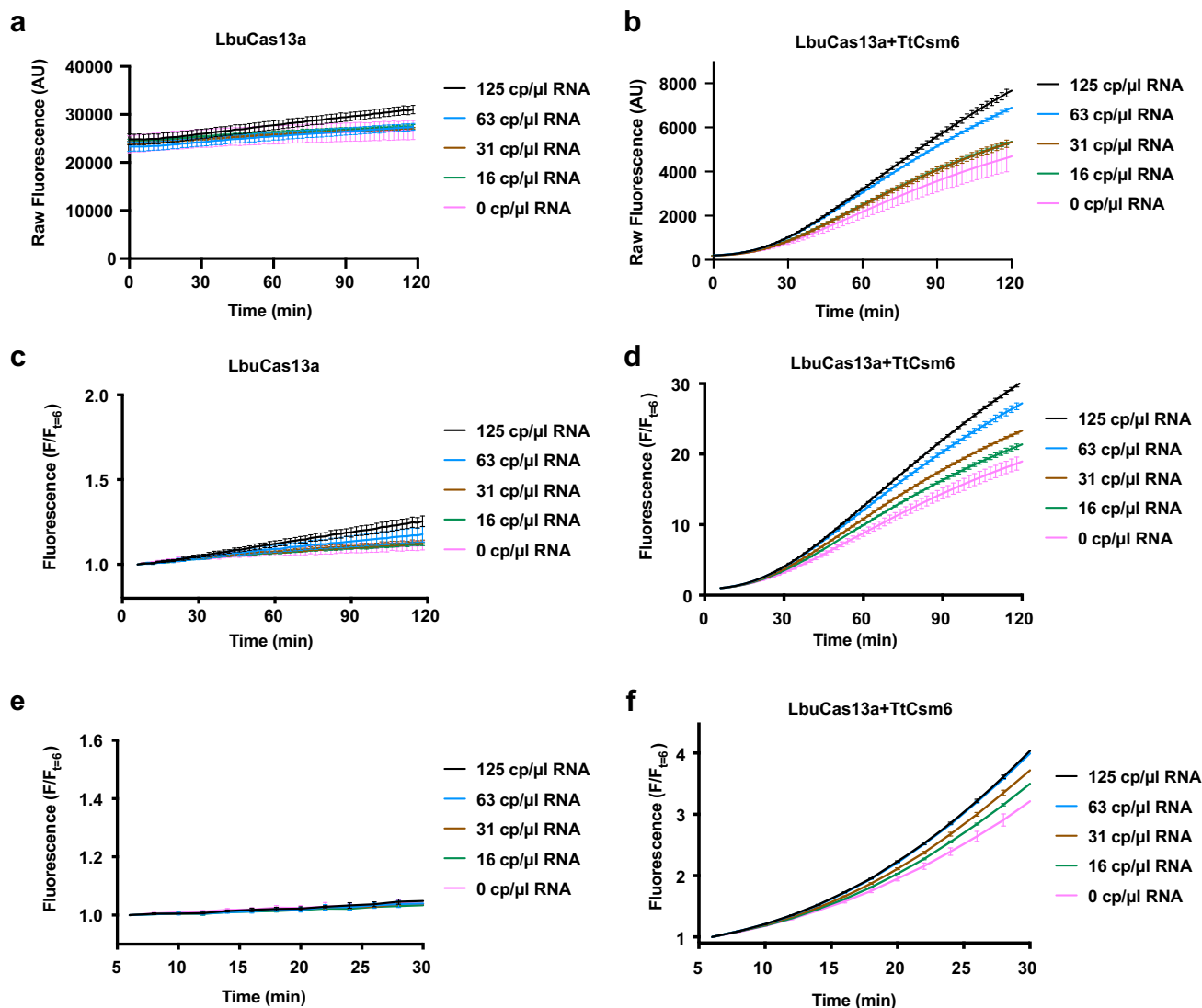
Extended Data Fig. 6 | Full time course data of LbuCas13a and LbuCas13a-TtCsm6 detection experiments in Fig. 3b,c. a) Raw fluorescence signal from LbuCas13a-mediated cleavage of a fluorescent reporter in the presence of 0-125 copies/μl (cp/μl) of B.E.I. SARS-CoV-2 RNA. LbuCas13a is complexed with eight crRNAs targeting the SARS-CoV-2 genome (604, 612, 542, 546, 564, 569, 588, 596). The mean raw fluorescence values (arbitrary units, AU) ± s.e.m. are plotted as lines with error bars ($n = 3$). These data are used for detection analysis in Fig. 3b at 20 min and 118 min. **b)** Raw fluorescence signal from an LbuCas13a-TtCsm6 detection assay containing 0-125 cp/μl B.E.I. SARS-CoV-2 genomic RNA. The same crRNAs were used as in **a**. The mean raw fluorescence values (arbitrary units, AU) ± s.e.m. are plotted as lines with error bars ($n = 3$). **c)** Graph of the data in **a**, but with measurements normalized to the fluorescence at t = 6 min. The mean normalized fluorescence values ($F/F_{t=6}$) ± S.E.M. are shown as lines with error bars ($n = 3$). **d)** Graph of the data in **b**, but normalized to the fluorescence at t = 6 min. The mean normalized fluorescence values ($F/F_{t=6}$) ± s.e.m. are shown as lines with error bars ($n = 3$). These data were used in Fig. 3c for detection analysis at 20 min and 118 min. **e)** Same dataset as in **c**, but zoomed to the first 30 min of the LbuCas13a assay. **f)** Same dataset as in **d**, but zoomed to the first 30 min of the LbuCas13a-TtCsm6 assay.

a 125 cp/µl

b 63 cp/µl

c 31 cp/µl

d 16 cp/µl

Replicates with target RNA ●———●

Control replicates (no target) ●———●

Extended Data Fig. 7 | Full time course data corresponding to the 20-replicate LbuCas13a-TtCsm6 detection experiments in Fig. 3d. a) 1-hour time course data for 20 replicates of FIND-IT reactions containing 125 copies per µl (cp/µl) of externally validated B.E.I. SARS-CoV-2 genomic RNA. Each set of 5 sample and 5 negative control (no target RNA) replicates were started simultaneously (R1-R5, R6-R10, R11-R15, R16-R20). Replicates with target RNA are plotted as black data points and lines, and control replicates lacking target RNA are plotted as pink data points and lines. Fluorescence was normalized to the fluorescence value at 6 min ($F/F_{t=6}$) to allow for temperature equilibration to 37 °C (See Extended Data Fig. 8). Each curve represents fluorescence data for a single replicate. **b)** As in **a**, but for sample reactions containing 63 cp/µl B.E.I. SARS-CoV-2 genomic RNA. **c)** As in **a**, but for sample reactions containing 31 cp/µl B.E.I. SARS-CoV-2 genomic RNA. **d)** As in **a**, but for sample reactions containing 16 cp/µl B.E.I. SARS-CoV-2 genomic RNA.
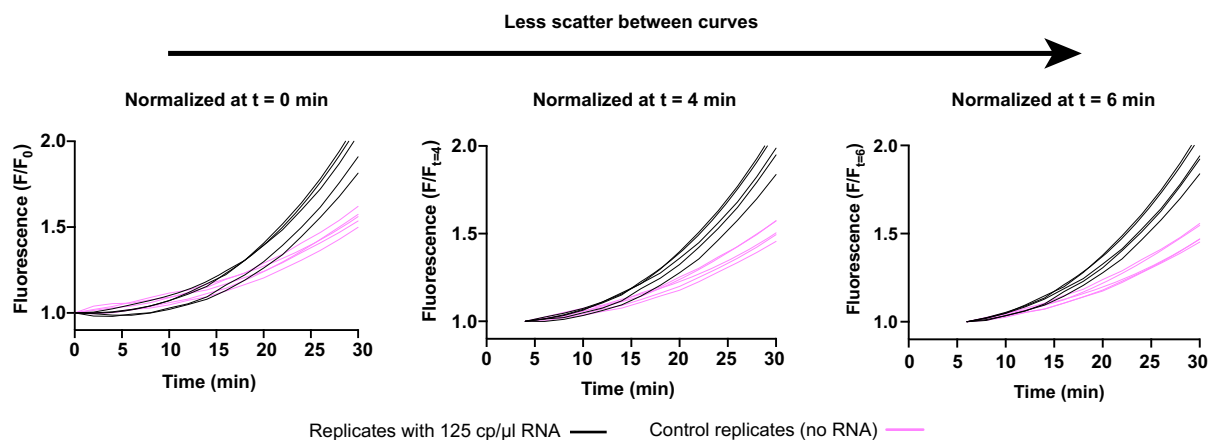
Extended Data Fig. 8 | Effect of normalizing fluorescence relative to different timepoints in a plate reader assay, related to Fig. 3. Graphs of 10 replicates from the LbuCas13a-TtCsm6 assay in Fig. 3d with LbuCas13a bound to eight crRNA sequences (604, 612, 542, 546, 564, 569, 588, 596), single-fluoro A_4-U_6 oligonucleotide, and 125 copies per μl (cp/μl) of B.E.I. SARS-CoV-2 genomic RNA as the target. Black curves indicate replicates containing RNA, and pink curves indicate control replicates lacking RNA. Comparison of the normalization at 0, 4, and 6 min (t = 0, 4, 6) shows that normalizing a few minutes after the start of the plate reader assay to allow for temperature equilibration reduces the effect of initial signal fluctuations on data normalization.
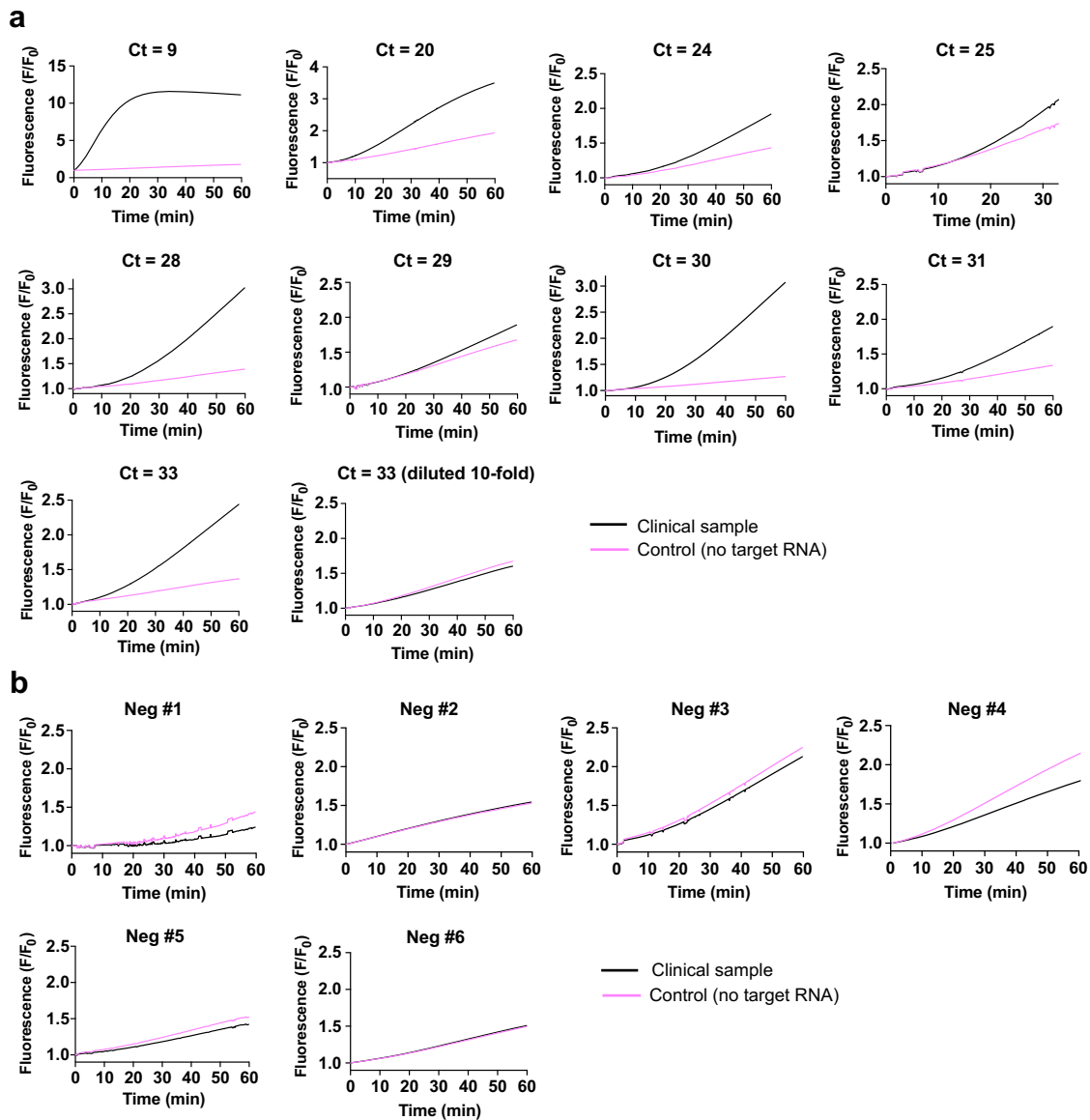
Extended Data Fig. 9 | Testing clinical samples with FIND-IT assay in a compact fluorescence detector, related to Fig. 4. a) Testing of SARS-CoV-2-positive clinical samples with FIND-IT using the compact detector in Fig. 4a–c. Images of the reaction wells were taken every 10 s for either 33 min (sample with a C_t value of 25) or 60 min (all other samples). Normalized fluorescence (F/F_0) of a sample reaction (black lines) and a control reaction run in parallel (pink lines) are plotted in each graph. C_t values for the *N* gene, *S* gene, and *ORF1ab* locus were previously determined by qRT-PCR in the IGI testing laboratory, and the average C_t value is shown for each sample tested (individual C_t values are provided in Supplementary Table 5). A reaction was also prepared in which a sample with a Ct value of 33 was diluted 10-fold in water prior to analysis ('Ct =33 (diluted 10-fold)'). **b)** As in **a**, but for clinical samples with C_t values > 37, which are considered negative for SARS-CoV-2, based on the qRT-PCR assay used by the IGI testing laboratory[30]. These data were used to determine the mean and s.d. of the fluorescence change of negative clinical samples (black) relative to their controls (pink; see Methods for details).
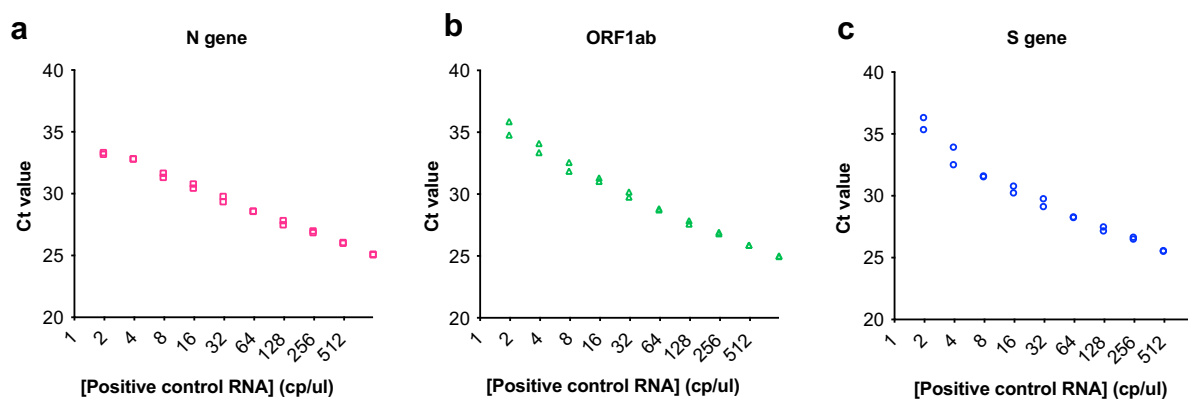
Extended Data Fig. 10 | Standard curve of qRT-PCR-derived C_t values versus sample RNA concentration. a) C_t values obtained from qRT-PCR for a dilution series of the positive control RNA provided by the Thermo TaqPath combo kit. The highest concentration of sample added to the reaction is 1000 copies per µl (cp/µl) and lower RNA concentrations were obtained by diluting the concentrated sample two-fold down to ~2 cp/µl. Primers for the *N* gene of SARS-CoV-2 were used for amplification. Two replicates for each concentration of RNA are plotted as pink squares. **b)** As in **a** but with primers for *ORF1ab* locus of SARS-CoV-2. Replicates are plotted as green triangles. **c)** As in **a** but with primers for the *S* gene of SARS-CoV-2. Replicates are plotted as blue circles.

nature research

Corresponding author(s):   Jennifer A. Doudna

Last updated by author(s):   Jun 14, 2021

Reporting Summary

Nature Research wishes to improve the reproducibility of the work that we publish. This form provides structure for consistency and transparency in reporting. For further information on Nature Research policies, see our Editorial Policies and the Editorial Policy Checklist.

Statistics

For all statistical analyses, confirm that the following items are present in the figure legend, table legend, main text, or Methods section.

n/a	Confirmed	
☐	☒	The exact sample size (*n*) for each experimental group/condition, given as a discrete number and unit of measurement
☐	☒	A statement on whether measurements were taken from distinct samples or whether the same sample was measured repeatedly
☐	☒	The statistical test(s) used AND whether they are one- or two-sided *Only common tests should be described solely by name; describe more complex techniques in the Methods section.*
☒	☐	A description of all covariates tested
☐	☒	A description of any assumptions or corrections, such as tests of normality and adjustment for multiple comparisons
☐	☒	A full description of the statistical parameters including central tendency (e.g. means) or other basic estimates (e.g. regression coefficient) AND variation (e.g. standard deviation) or associated estimates of uncertainty (e.g. confidence intervals)
☐	☒	For null hypothesis testing, the test statistic (e.g. F, t, r) with confidence intervals, effect sizes, degrees of freedom and P value noted *Give P values as exact values whenever suitable.*
☒	☐	For Bayesian analysis, information on the choice of priors and Markov chain Monte Carlo settings
☒	☐	For hierarchical and complex designs, identification of the appropriate level for tests and full reporting of outcomes
☒	☐	Estimates of effect sizes (e.g. Cohen's *d*, Pearson's *r*), indicating how they were calculated

Our web collection on statistics for biologists contains articles on many of the points above.

Software and code

Policy information about availability of computer code

Data collection	Plate reader data was collected using a Tecan Spark or Biotek plate reader and data were exported to Microsoft Excel. Clinical sample data was collected using a custom compact detector system that is described in the manuscript; custom control of the imaging hardware for the compact detector was implemented in MATLAB (2020a), using Thorlabs drivers and SDK (ThorCam) to control the camera acquisition, and serial communication to an Arduino Bluefruit Feather board to electronically trigger LED illumination. Oligonucleotide samples treated with TtCsm6 were analyzed using a Synapt G2-Si mass spectrometer that was equipped with an electrospray ionization (ESI) source and a BEH C18 ionKey (length: 50 mm, inner diameter: 150 μm, particle size: 1.7 μm, pore size: 130 Å), and connected in line with an Acquity M-class ultra-performance liquid chromatography system (UPLC; Waters, Milford, MA). Mass spectrometry data acquisition was performed using MassLynx software (version 4.1, Waters). qRT-PCR data in Extended Data Fig. 10 was collected on a QuantStudio 6 Real-Time PCR System (ThermoFisher Scientific).
Data analysis	Data was analyzed using MATLAB (2020a), Graphpad Prism (version 9.1.2), Python (version 3.8.1), and Microsoft Excel for Mac (version 16.50) Mathematical modeling of the Cas13-Csm6 reaction was done in Mathematica 12 (Wolfram). All custom data analysis for limit of detection analysis for 20-replicate experiments, and the code used for mathematical modeling of the Cas13-Csm6 reaction and illumination correction of images is available at: https://github.com/jackdesmarais/FIND-IT. An archived version is available at: http://doi.org/10.5281/zenodo.492192441 (Citation: Desmarais, J. J., & Bhuiya, A. jackdesmarais/FIND-IT-paper: v1.0 (Version paper_code). Zenodo (2021). http://doi.org/10.5281/zenodo.4921924) Adobe Photoshop 2021 (v. 22.1.1) was used to adjust the tone, brightness, and contrast of images in Fig. 4d. Mass spectrometry data processing was performed using MassLynx software (version 4.1, Waters). qRT-PCR data was analyzed using the QuantStudio 6 Design & Analysis software, v4.2.3 (ThermoFisher Scientific).

For manuscripts utilizing custom algorithms or software that are central to the research but not yet described in published literature, software must be made available to editors and reviewers. We strongly encourage code deposition in a community repository (e.g. GitHub). See the Nature Research guidelines for submitting code & software for further information.

Data

Policy information about availability of data

All manuscripts must include a data availability statement. This statement should provide the following information, where applicable:

- Accession codes, unique identifiers, or web links for publicly available datasets
- A list of figures that have associated raw data
- A description of any restrictions on data availability

Data that support the findings of this study are provided in the Source Data files for each figure (Figs. 1-4, and Extended Data Figs. 1, 3-10). The plasmid used to express MBP-tagged LbuCas13a (p2CT-His-MBP-Lbu_C2c2_WT) is available from Addgene (83482). Plasmids used for expression of SUMO-tagged LbuCas13a (pGJK_His-SUMO-LbuCas13a), His-tagged EiCsm6 (pET28a_His-TEV-EiCsm6) and His-SUMO-tagged TtCsm6 (pET_His6-SUMO-TEV-TtCsm6) will be deposited in Addgene upon publication (172488, 172487, and 172486). Sequences of RNA oligonucleotides are provided in Supplementary Table 3.

Field-specific reporting

Please select the one below that is the best fit for your research. If you are not sure, read the appropriate sections before making your selection.

[x] Life sciences   [ ] Behavioural & social sciences   [ ] Ecological, evolutionary & environmental sciences

For a reference copy of the document with all sections, see nature.com/documents/nr-reporting-summary-flat.pdf

Life sciences study design

All studies must disclose on these points even when the disclosure is negative.

Sample size	No sample size calculations were performed. Plate reader experiments included 3 replicates for every condition in order to determine the mean and standard error or confidence interval. The sample size in plate reader experiments was limited by the number of the reactions that could be started close together in time using an 8-well or 12-well multichannel pipette (e.g. 20-replicate experiments were run in 2 groups of 10, with five controls and five positive samples per group). The number of clinical samples tested with FIND-IT on the compact detector was limited by the number and volume of individual samples obtained from the IGI testing lab, and also limited by equipment availability. Nine COVID-19 positive samples spanning a wide range of Ct values (9-33) were tested to see if FIND-IT could be used to detect extracted viral RNA from patient samples. Six COVID-19 negative samples were tested to determine of the mean and standard deviation of the clinical negative samples.
Data exclusions	Initial three time points of plate reader runs (0-4 min) were excluded from normalization analysis for Fig. 3c, Fig. 3d, Extended Data Fig. 6c-f, Extended Data Fig. 7a-d (where fluorescence was normalized to F at t = 6 min). This allows the temperature to equilibrate to 37°C for a few minutes at the start of each plate assay. The improved signal-to-noise of this normalization is shown in Extended Data Fig. 8. Full raw datasets used to generate all normalized curves are also provided in the associated Source data files for each figure.
Replication	All plate reader experiments were performed in triplicate or with 20 replicates as indicated in the figures, and several 20-replicate and triplicate datasets were repeated by different individuals for additional confirmation of reproducibility/robustness. qRT-PCR experiments to determine the correlation of RNA concentration with Ct value was performed with two replicates. Clinical samples were run once due to insufficient sample volume for more runs.
Randomization	No randomization was performed. Sample and control reactions for biochemical experiments were assembled with the same reagents and volumes, and were measured at the same time in the plate reader or compact detector when making direct comparisons to a control.
Blinding	No blinding was performed, as it was necessary to know which reaction had target RNA and which reactions contained controls in order to set up the biochemical reactions testing the detection sensitivity, speed, and accuracy of our assay.

Reporting for specific materials, systems and methods

We require information from authors about some types of materials, experimental systems and methods used in many studies. Here, indicate whether each material, system or method listed is relevant to your study. If you are not sure if a list item applies to your research, read the appropriate section before selecting a response.

Materials & experimental systems

n/a	Involved in the study
[x]	[ ] Antibodies
[x]	[ ] Eukaryotic cell lines
[x]	[ ] Palaeontology and archaeology
[x]	[ ] Animals and other organisms
[x]	[ ] Human research participants
[x]	[ ] Clinical data
[x]	[ ] Dual use research of concern

Methods

n/a	Involved in the study
[x]	[ ] ChIP-seq
[x]	[ ] Flow cytometry
[x]	[ ] MRI-based neuroimaging